

**CASTLE MOUNTAIN  
GEOTECHNICAL FEASIBILITY REPORT**

*Prepared for*  
EQUINOX GOLD CORP.

*By*  
Call & Nicholas, Inc.

April 2020

**CALL & NICHOLAS, INC.**

**REVISION HISTORY**

| Revision | Date          | Description                  |
|----------|---------------|------------------------------|
| 00       | April 2020    | Initial release.             |
| 01       | February 2022 | Revised issue with PE stamp. |

## Professional Certification

Call & Nicholas, Inc. (CNI) is pleased to present this geotechnical study to Equinox Gold Corp (EQX). This study was conducted in accordance with a proposal submitted by CNI to EQX on 01 November 2019 and reviewed by Mr. Scott Cylwik, a California registered Professional Engineer. This study builds upon the *2017 Pre-feasibility Slope Stability Report for the Castle Mountain Reserve Pits* report by CNI and presents slope angle recommendations based on the known and provided data at the time of this report. As more information becomes available and pit designs change, the recommended and achievable slope angles may need to be updated to reflect the conditions.

Thank you for the opportunity and we look forward to assisting you in the future.

Sincerely,

Call & Nicholas, Inc.

Scott Cylwik, California P.E. 85060

Senior Engineer

## TABLE OF CONTENTS

|            |  |            |
|------------|--|------------|
| <b>1.0</b> | <b>EXECUTIVE SUMMARY .....</b>   | <b>1-1</b> |
| 1.1        | RECOMMENDED INTERRAMP SLOPE ANGLES FOR THE CASTLE MOUNTAIN PITS.....                           | 1-1        |
| 1.2        | BASIS FOR RECOMMENDATIONS.....   | 1-3        |
| 1.3        | RECOMMENDED FUTURE WORK.....   | 1-4        |
| <b>2.0</b> | <b>INTRODUCTION.....</b>   | <b>2-1</b> |
| <b>3.0</b> | <b>ENGINEERING GEOLOGY .....</b>   | <b>3-1</b> |
| 3.1        | GEOLOGIC STRUCTURE.....  | 3-2        |
| 3.2        | FAULTS IDENTIFIED AT THE CASTLE MOUNTAIN MINING PROPERTY .....                                 | 3-3        |
| 3.3        | ROCK FABRIC – CELL MAPPING .....   | 3-4        |
| 3.4        | ROCK FABRIC – TELEVIEWER DATA .....  | 3-4        |
| 3.4.1      | <i>Geomechanical Logging</i> .....   | 3-5        |
| <b>4.0</b> | <b>LABORATORY TESTING AND ROCK-MASS STRENGTHS.....</b>   | <b>4-1</b> |
| 4.1        | SPATIAL ROCK QUALITY .....   | 4-2        |
| 4.2        | FRACTURE SHEAR STRENGTH .....  | 4-3        |
| 4.3        | WEAK CLAY-ALTERED MATERIAL STRENGTH .....  | 4-4        |
| 4.3.1      | <i>Remolded Direct Shear Tests on Clay Samples</i> .....                                       | 4-4        |
| 4.3.2      | <i>Back-Analyzed Clay Strengths</i> .....  | 4-5        |
| 4.4        | INTACT ROCK STRENGTH TESTING .....   | 4-7        |
| 4.4.1      | <i>Intact Shear Strength Based on Uniaxial Compressive Strength and Tensile Strength</i> ..... | 4-7        |
| 4.5        | ROCK-MASS STRENGTHS .....  | 4-8        |
| 4.5.1      | <i>CNI Rock-Mass Strength Estimation Method</i> .....  | 4-9        |
| 4.5.2      | <i>Comparison of CNI and Hoek-Brown Rock-Mass Strength Estimation Methods</i> .....            | 4-10       |
| <b>5.0</b> | <b>BENCH DESIGN.....</b>   | <b>5-1</b> |
| 5.1        | EXAMPLE OF ESTIMATING BENCH FACE ANGLE IN SW WALL OF CASTLE MOUNTAIN PITS ..                   | 5-2        |
| 5.2        | CATCH-BENCH WIDTH .....  | 5-3        |
| 5.3        | CATCH-BENCH DESIGN .....   | 5-4        |
| <b>6.0</b> | <b>OVERALL SLOPE ANALYSIS .....</b>  | <b>6-1</b> |
| 6.1        | MODEL INPUT PARAMETERS .....   | 6-1        |
| 6.1.1      | <i>Geology Model</i> .....   | 6-1        |
| 6.1.2      | <i>Material Properties</i> .....   | 6-2        |
| 6.1.3      | <i>Hydrogeology</i> .....  | 6-2        |
| 6.2        | RESULTS .....  | 6-2        |
| 6.2.1      | <i>Section 1</i> .....   | 6-3        |
| 6.2.2      | <i>Section 2</i> .....   | 6-3        |
| 6.2.3      | <i>Section 3</i> .....   | 6-4        |

|            |   |            |
|------------|---|------------|
| 6.2.4      | Section 4.....  | 6-4        |
| 6.2.5      | Section 5.....  | 6-4        |
| 6.2.6      | Section 6.....  | 6-5        |
| 6.2.7      | Section 7.....  | 6-5        |
| 6.2.8      | Section 8.....  | 6-5        |
| 6.2.9      | Section 9.....  | 6-6        |
| 6.2.10     | Section 10.....                                       | 6-6        |
| 6.2.11     | Section 11.....                                       | 6-6        |
| 6.2.12     | Section 12.....                                       | 6-6        |
| 6.2.13     | Section 13.....                                       | 6-7        |
| 6.2.14     | Section 14.....                                       | 6-7        |
| 6.2.15     | Section 15.....                                       | 6-7        |
| <b>7.0</b> | <b>BLASTING OPERATIONS .....</b>                      | <b>7-1</b> |
| 7.1        | PRODUCTION BLASTING .....                             | 7-1        |
| 7.2        | CONTROLLED BLASTING .....                             | 7-1        |
| 7.2.1      | <i>Initial Pre-Split Blasting Recommendation.....</i> | <i>7-2</i> |
| 7.2.2      | <i>Initial Buffer Blasting Recommendation.....</i>    | <i>7-3</i> |
| 7.2.3      | <i>Controlled Blast Audits .....</i>                  | <i>7-5</i> |

*Appendices*

|                   |  |
|-------------------|--|
| <i>Appendix A</i> | <i>RQD Block Model Release Notes</i>   |
| <i>Appendix B</i> | <i>1993 and 2017 CNI Cell Mapping</i>  |
| <i>Appendix C</i> | <i>2019 Televiewer Data</i>            |
| <i>Appendix D</i> | <i>2019 Geomechanical Data</i>         |
| <i>Appendix E</i> | <i>Rock Strength Data</i>              |
| <i>Appendix F</i> | <i>X-Ray Diffraction Results</i>       |
| <i>Appendix G</i> | <i>Modeled Bench Face Angle Curves</i> |

## LIST OF TABLES

|           |   |
|-----------|---|
| Table 1-1 | Generic Recommended Interramp Slope Angles                          |
| Table 1-2 | Domain-Specific Recommended Interramp Slope Angles                  |
| Table 1-3 | Bench Design Parameters   |
| Table 3-1 | Average RQD and GSI Values by Rock Type                             |
| Table 4-1 | Laboratory Testing Manifest   |
| Table 4-2 | 30th Percentile RQD Values at Different Distances from Major Faults |
| Table 4-3 | Fracture Shear Strengths  |
| Table 4-4 | Remolded Clay Direct Shear Strengths                                |
| Table 4-5 | Intact Strength Summary   |
| Table 4-6 | Rock-Mass Strength Estimates  |
| Table 5-1 | Bench Scale Analysis Results  |
| Table 6-1 | Overall Stability Analyses Results                                  |

## LIST OF FIGURES

- Figure 1-1 Recommended Domain Boundaries on 2019 Preliminary Pit Design
- Figure 3-1 Exposed Geology on 2019 Preliminary Pit Design
- Figure 3-2 Fault Data from Capps 1991 and CNI 1993/2017
- Figure 3-3 Exposed Faults on 2019 Preliminary Pit Design
- Figure 3-4 Cell Mapping Data from 2017 and 1993
- Figure 3-5 2017 and 1993 Cell Mapping Locations
- Figure 3-6 20200203 Design Drill Holes Map
- Figure 3-7 GT-001
- Figure 3-8 GT-002
- Figure 3-9 GT-003
- Figure 3-10 GT-004
- Figure 3-11 All Joints
- Figure 3-12 All Faults
- Figure 3-13 Andesite Structures
- Figure 3-14 Autoclastic Structures
- Figure 3-15 Epiclastic Structures
- Figure 3-16 Rhyolite Structures
- Figure 3-17 Volcaniclastic Structures
- Figure 3-18 Downhole Plots of RQD and GSI
- Figure 3-19 Down Hole Bar Charts of Core Quality
- Figure 3-20 Cumulative Frequency RQD Plots for Each Formation
- Figure 4-1 Epiclastic and Andesite Drillhole RQD Distribution
- Figure 4-2 Volcaniclastic and Rhyolite Drillhole RQD Distribution
- Figure 4-3 Relationship between Friction Angle and Cohesion of Clay Materials
- Figure 4-4 Empirical Correlations to GSI
- Figure 4-5 Rock-Mass Strength Comparison for Moderate Andesite
- Figure 5-1 Number of Spaces of Control Joint Broken to Achieve the Measured Bench Face Angle as a Function of the Average Control Joint Spacing
- Figure 5-2 Log-Log Plot of Number of Control Joint Spaces Broken to Achieve the Measured Bench Face Angle as a Function of the Average Control Joint Spacing

## LIST OF FIGURES (Continued)

- Figure 5-3 Log-Log Plot of Number of Control Joint Spaces Broken to Achieve the Measured Bench Face Angle as a Function of the Average Spacing x Length x the Angle to the Strike of the Bench Face
- Figure 5-4 Definition of Back Break
- Figure 5-5 Blast Damage Comparison between Pre-Split Perimeter and Trim Row Perimeter Blasting
- Figure 5-6 Blast Damage Curve for the South and Southwest Walls Measured in the JSLA and OBHT Pits
- Figure 5-7 Modeled Bench Face Angle Distributions for Southwest Slope with a Slope Direction of 45 Degrees
- Figure 5-8 80-Percent Reliability Bench Face Angles as a Function of Slope Dip Direction
- Figure 5-9 Example Bench Face Angle Distribution with 80-Percent Reliability
- Figure 6-1 Slope Stability Cross Sections on 2019 Preliminary Pit Design
- Figure 6-2 Geologic Section 1 (Looking North) Designed Pit
- Figure 6-3 Geologic Section 1 (Looking NE) Optimized Pit
- Figure 6-4 Geologic Section 2 (Looking NE) Designed Pit
- Figure 6-5 Geologic Section 2 (Looking NE) Optimized Pit
- Figure 6-6 Geologic Section 3 (Looking NE) Designed Pit
- Figure 6-7 Geologic Section 3 (Looking NE) Optimized Pit
- Figure 6-8 Geologic Section 4 (Looking NW) Designed Pit
- Figure 6-9 Geologic Section 4 (Looking NW) Optimized Pit
- Figure 6-10 Geologic Section 5 (Looking South) Designed Pit
- Figure 6-11 Geologic Section 5 (Looking South) Optimized Pit
- Figure 6-12 Geologic Section 6 (Looking SE) Designed Pit
- Figure 6-13 Geologic Section 6 (Looking SE) Optimized Pit
- Figure 6-14 Geologic Section 7 (Looking NW) Designed Pit
- Figure 6-15 Geologic Section 7 (Looking NW) Optimized Pit
- Figure 6-16 Geologic Section 8 (Looking NE) Designed Pit
- Figure 6-17 Geologic Section 8 (Looking NE) Optimized Pit
- Figure 6-18 Geologic Section 9 (Looking South) Designed Pit
- Figure 6-19 Geologic Section 9 (Looking South) Optimized Pit
- Figure 6-20 Geologic Section 10 (Looking SW) Designed Pit

## **LIST OF FIGURES (Continued)**

- Figure 6-21 Geologic Section 10 (Looking SW) Optimized Pit
- Figure 6-22 Geologic Section 11 (Looking East) Designed Pit
- Figure 6-23 Geologic Section 11 (Looking East) Optimized Pit
- Figure 6-24 Geologic Section 12 (Looking North) Designed Pit
- Figure 6-25 Geologic Section 13 (Looking South) Designed Pit
- Figure 6-26 Geologic Section 13 (Looking South) Optimized Pit
- Figure 6-27 Geologic Section 14 (Looking NE) Designed Pit
- Figure 6-28 Geologic Section 14 (Looking NE) Optimized Pit
- Figure 6-29 Geologic Section 15 (Looking NE) Designed Pit
- Figure 6-30 Geologic Section 15 (Looking NE) Optimized Pit
- Figure 7-1 Differential Tonnage Between 40- and 45- degree Interamp Slope Angles and Cost of Pre-splitting as a Function of Interramp Slope Height
- Figure 7-2 Preliminary Pre-Split and Butter Blast Layout - 52° ISA
- Figure 7-3 Benefit of Pre-Split Blasting at a Mine in Chile with a Good Quality Rock Mass

## 1.0 EXECUTIVE SUMMARY

As requested by Equinox Gold Corp. (EQX), Call & Nicholas, Inc. (CNI) performed a slope stability study for the Castle Mountain project based on preliminary pit designs provided by John Nilsson. The purpose of this study was primarily to update recommended design interramp slope angles and bench design parameters based on new laboratory testing, new geomechanical drilling information, and an updated geologic model.

Overall analytical stability analyses were conducted on key areas of the preliminary pits with updated rock-mass strengths. The rock-mass strengths were derived from the new laboratory testing and applied to zones of similar geology. An updated 3D geologic model was provided by EQX geologists. A rock quality block model using the rock quality designation parameter (RQD) was generated by CNI as part of this study. The model release notes are attached as *Appendix A - RQD Block Model Release Notes*.

### 1.1 Recommended Interramp Slope Angles for the Castle Mountain Pits

Figure 1-1 shows the locations of the recommended domain boundaries with interramp slope angles (ISA). Table 1-1 reports the recommended interramp slope angles resulting from the analyses listed above.

**Table 1-1. Generic Recommended Interramp Slope Angles**

| Domain           | ISA (deg) |                |            |          |
|------------------|-----------|----------------|------------|----------|
|                  | Rhyolite  | Volcaniclastic | Epiclastic | Andesite |
| ISA_GENERIC_SD   | 51        | 50             | 50         | 48       |
| ISA_GENERIC_WEST | 51        | 50             | 50         | 48       |
| ISA_GENERIC_EAST | 52        | 52             | 52         | 52       |

Zones around key fault geometries were identified as having potentially weak altered rock. Many of the instabilities that occurred in the Oro Belle and JSLA pits were attributed to this weak altered material and the unfavorable geometry in relation to the pit walls. Table 1-2 shows the recommended interramp slope angles for the zones around the major faults. The “ISA\_ISLAND” domain is a special case where there is an intersection of multiple faults and associated highly altered zones. An overall slope stability model indicates that this area is unstable and will require remediation if left in the design. With the proposed design that was analyzed, removing the material above the 4040 elevation would be sufficient.

**Table 1-2. Domain-Specific Recommended Interramp Slope Angles**

| <b>Domain</b>           | <b>ISA (deg)</b> | <b>Perpendicular Range</b> |
|-------------------------|------------------|----------------------------|
| ISA_DILLON_FAULT        | 40               | ±100ft                     |
| ISA_MCLANE_FAULT        | 40               | ±200ft                     |
| ISA_MAVERICK_WEST_FAULT | 46               | ±200ft                     |
| ISA_PREDATOR_FAULT      | 46               | ±200ft                     |
| ISA_ISLAND              | Complete Removal |                            |

The catch bench design criteria are presented in Table 1-3. The analytical results from the catch bench analyses have not been updated since the 2017 report but catch bench designs have been updated to reflect the updated ISA recommendations. The catch bench designs summarized in Table 1-3 assume high quality controlled blasting practices with single pass pre-split blasting over the entire triple bench height of 60 feet. If the as-mined catch benches do not consistently achieve the required 27-foot width (after blasting, excavation, and scaling), then either blasting and mining practices should to be improved or the ISA would need to be reduced. The as-mined bench geometries should be verified with either optical scans or drone scans to verify bench performance.

**Table 1-3. Bench Design Parameters**

| <b>Domain</b>                                 | <b>ISA (deg)</b> | <b>Geology</b>               | <b>Design BFA (deg)</b> | <b>Design Bench Height (ft)</b> | <b>Design Bench Width (ft)</b> |
|---|------------------|------------------------------|-------------------------|---------------------------------|--------------------------------|
| ISA_GENERIC_EAST                              | 52               | All                          | 79                      | 60                              | 35                             |
| ISA_GENERIC_WEST<br>ISA_GENERIC_SD            | 51               | Rhyolite                     | 74                      | 60                              | 31                             |
|   | 50               | Volcaniclastic<br>Epiclastic | 74                      | 60                              | 33                             |
|   | 48               | Andesite                     | 74                      | 60                              | 37                             |
| ISA_DILLON_FAULT<br>ISA_MCLANE_FAULT          | 40               | All                          | 60                      | 60                              | 37                             |
| ISA_MAVERICK_WEST_FAULT<br>ISA_PREDATOR_FAULT | 46               | All                          | 65                      | 60                              | 30                             |

In addition to the recommended interramp slope angles, a crest offset of 300 feet is recommended for infrastructure that will be constructed on the western side of the South Extension pit. Stability analyses indicate that the location and orientation of the Maverick fault could potentially lead to instability within 300 feet of the crest. This recommendation is based

on adding an anisotropy equal to the properties of the fault applied throughout the rock mass. If the fault is accurately modeled and does not deviate significantly from its modeled location, the slope is stable with current estimations. By allowing the fault to “move” throughout the rock mass, a safe distance behind the crest can be estimated where the modeled slip surface has a factor of safety (FOS) of at least 1.2.

## **1.2 Basis for Recommendations**

Slope angles are recommended based on a combination of overall, interramp, and bench-scale stability concerns. Each component requires specific data that is refined and optimized as the project matures. As part of the prefeasibility study conducted in 2017, the interramp and bench-scale stability models were run with an adequate data set, but rock-mass strengths and the spatial application of the strengths was poorly defined for the overall stability analyses. This study focuses on further characterization of the rock mass and overall stability concerns.

Additionally, the overall stability analyses performed to complete this study assumed dry conditions and dewatering the slopes is critical to achieve the recommended angles.

## **1.3 Controlled Blasting on Final Wall**

The recommended slope angles assume that controlled blasting will be performed, in particular on the final walls of the design. If controlled blasting is not performed, the recommendations will need to be updated to account for increased blast damage of the bench faces. Controlled blasting techniques include utilizing trim shots, buffer rows, pre-split blasting, always blasting to a free face, and not drop cutting next to the final wall. In addition to constructing clean, well-cut bench faces, the reliability of catch benches can be improved by ensuring the toes of each mining increment are cleaned before proceeding with the next increment. Leaving material that can be easily cleaned is not good practice because it reduces the capacity of the bench to catch falling rock and also interferes with the drill’s ability to reach the toe of the current bench on the second double-bench increment. Drilling the final row of holes against the bench face to the full triple-bench height of 60 feet improves the reliability of the benches by increasing achieved bench-face angles

## **1.4 Uncertainty Regarding Clay Zones**

Many of the previous slope instabilities that have occurred at Castle Mountain were

attributed to weak clay altered material combined with an unfavorable geometry in relation to the pit walls. Zones around key fault geometries were identified as having potentially weak altered rock in this study. However, current drilling coverage is relatively poor within the final walls of the proposed design. Therefore, some instability should be expected if unanticipated clay zones are intercepted. This risk can be remediated and reduced by drilling geotechnical core holes on 500-foot centers throughout the final walls of the proposed mine design.

### **1.5 Recommended Future Work**

1. Slope design is an iterative process; optimum slope design requires continuous effort to collect, interpret, and analyze geologic and geotechnical data as they become available. When the mine plan with ramps is completed, a second series of overall analyses should be undertaken to optimize interramp slope angles. Updated mine designs should be reviewed and evaluated for geotechnical design compliance and, if necessary, slope stability before they are implemented.
2. Groundwater conditions are an important component for slope stability analyses. For the overall analysis performed herein, CNI assumed depressurized conditions. CNI recommends having a complete hydrological study completed that defines and models the regional in situ groundwater conditions. If pore pressures are anticipated within the final pit walls, the overall stability analyses will need to be updated with that information. Additionally, potential dewatering measures must be developed should it be necessary to lower water pressures to improve stability.
3. Optical drone scans of the constructed bench-face angles should be performed routinely to evaluate catch-bench width performance. These surveys utilize scans of as-mined bench faces to evaluate the success rate of achieving the designed bench and interramp geometries; it is important to collect scan data for all wall orientations. These data should be collected in all active mining areas and are used to calibrate bench-scale slope analysis and further refine the slope design template.
4. Reduction of triaxial tests yielded unrealistic intact rock strengths and a correlation between uniaxial and disk tension were used. Additional triaxial testing on all major rock units is recommended to further characterize the intact strength of materials.
5. CNI recommends starting a robust slope monitoring program to capture long-term trends of potential slope deformation. Installing optical prisms on benches as mining progresses is a best practice to maintain monitoring as benches may become inaccessible in the future.
6. CNI also recommends that intermediate and minor faults and intense clay altered zones should be modeled with up-to-date geologic bench maps. This mapping and modeling are continuous processes and key to mitigation of unstable areas and to provide input to design changes to maximize ore recovery in every design phase.
7. All core drilling should be geomechanically logged to update the geotechnical block models of rock quality, clay alteration, and rock hardness within each of the defined

- geologic units. Drillholes located near and behind the final pit wall are critical for characterizing the rock mass.
8. Vibrating wire piezometers should be installed in stacked profiles in several holes in various locations of the mine to determine pore pressure gradients and how mining impacts the gradients over time. This will provide needed data for coupled geotechnical and hydrogeologic models to determine if groundwater will have an impact on the overall stability of the pits. This is especially true in the South Extension area where previous studies indicate a water table may exist at the 3900-foot elevation.

## 2.0 INTRODUCTION

At the request of Mr. Travis O'Farrell of Equinox Gold Corp. (EQX), Call & Nicholas, Inc. (CNI) conducted a slope stability analysis for the Castle Mountain Project, located in California, approximately 15 miles southwest of Searchlight, Nevada. The purpose of this study was to provide slope angles for a feasibility level study based on available data. Preliminary pit designs provided by John Nilsson on February 3, 2020 were used as for the basis of the study.

Data available for this study included the following:

1. CNI conducted field mapping to identify and measure geologic structural trends in the rock fabric and collected clay samples for laboratory testing as part of the 2017 prefeasibility study.
2. The rock fabric data collected in 2017 was combined with data originally collected by CNI in 1993 for the JSLA pit slope study. This data was used to analyze the bench-scale stability. Bench design recommendations for this study were based on these previous studies.
3. The major structure data used included Capps 1991 mapping in the JSLA pit. The major structure data was digitized and used to estimate the fault length, spacing, and orientation statistics for use in the interramp stability analysis in the 2017 prefeasibility study.
4. Clay strengths were estimated for use in the overall stability analysis based on laboratory samples collected from the field mapping and back-analyses from three previous failures that occurred at the property.
5. An RQD block model was created based on the available geomechanical drill data and was used to study the spatial relationship of rock quality.
6. Geomechanical measurements and laboratory samples were collected from four geotechnical drill holes. Data were logged and collected by CNI personnel.
7. Small scale direct shear, uniaxial compressive strength, triaxial compressive strength, and disk tension laboratory tests were conducted on samples obtained as part of the geotechnical drilling campaign.

### 2.1 Personnel

Mr. Ross Barkley, Vice President, is responsible for the technical direction and review of all project work. Mr. Scott Cylwik, Senior Engineer (California P.E. #85060), reviewed the work in February 2022 to confirm that the methods and practices meet California standards.

Various CNI engineers and geologists participated in data collection and analytical work. Mr. Sean DeBruin collected cell mapping data and materials to be tested in the laboratory. Mr. Daniel Childs collected cell mapping data, materials for laboratory testing, estimated rock mass

strengths, and ran 2D limit equilibrium models on the provided pit geometry. Mr. Ross Barkley ran the bench-scale stability analysis and oversaw all technical work.

### 3.0 ENGINEERING GEOLOGY

This geology summary is a brief compilation of work performed by previous owners of the property and their consulting geologists, including reports published by Capps and Moore (1991, 1994, and 1997); and Linder (1989). In particular, the rock types, alteration types, and structural patterns are important to the analysis of the stability of mined rock slopes.

Rocks that will be exposed in the slopes of the Castle Mountain project pits were deposited during a period of intense volcanism starting in the Miocene (18.5 Ma). This period of volcanism lasted roughly 5 million years and finished with the deposition of the Piute Range volcanics at 13.5 Ma. The sequence of rocks that will be exposed in the proposed pits is referred to as the Castle Mountains Volcanic (CMV) sequence. This sequence includes the Jacks Well volcanics (trachyandesite and basalt, 18.5 to 15.2 Ma), the Linder Peak volcanics (rhyolite flow domes and tuffs, 15 Ma), and the Hart Peak (rhyolite plugs, flows and trachydacite intrusions, 15 to 14 Ma). The updated geologic model provided by EQX is exposed on the preliminary pit designs and presented in Figure 3-1.

The alteration is described as typical of high-level epithermal systems. Ore mineralization is associated with silicification grading outward to argillic, propylitic, and unaltered rock. Of particular importance is the distribution of the argillic alteration zones. Samples of intensely clay altered rocks were collected from the west wall of the Oro Belle Pit and indicate that the major clay is a mixed layer illite and smectite. Multiple bench failures that occurred during mining in the 1990s and early 2000s in the Jumbo North and Oro Belle pits were related to significant volumes of this weak material. The upper east wall of the Oro Belle pit experienced a roughly 200-kiloton failure in clay altered agglomerate-lapilli-tuff. The wall was originally excavated at a 52-degree interramp slope angle that failed at an overall wall height of 260 feet. The wall was remediated to a stable configuration at a 33-degree interramp slope angle.

Another failure related to weak clay altered material occurred on the northwest wall of the Jumbo North pit. This failure was associated with a northeast striking, steeply SE dipping fault that acted as a backplane release to the failure. The weak clay-altered rock mass between the toe of the slope at the 4000-foot elevation and the fault backplane was not strong enough to overcome the driving forces of the 220-foot high slope that was excavated at a 53-degree angle.

Non-daylighted wedge failures also occurred in the east wall of the Jumbo North pit. Again, a weak clay altered material constituted the rock mass between the non-daylighted wedge release and the toe of the slope. The rock mass was not strong enough to withstand the driving forces of the 59-degree interramp angle for the 240-foot high slope.

Because all the failures experienced within the Castle Mountain pits have been associated with the weak clay altered materials, the location of these units is of paramount importance for slope stability. Working with EQX geologists, the current understanding is that the weak clay altered materials are in close vicinity of major mapped faults. Drillhole data indicate that there are other areas with the weak clay altered material not associated with the major mapped faults, but there is not a current model indicating where these units exist. Bench mapping will be key in identifying the extent of these clay bodies in the early phases of mining, and whether they are important in the overall stability of the designs.

### **3.1 Geologic Structure**

Geologic structure, including faults, joints, bedding, and lithologic contacts, are weaknesses within the rock that must be identified and analyzed to design appropriate pit slope angles. These structures impact the rock-mass strength, provide major boundary releases to daylighted and non-daylighted failures, and impact the bench face angles that can be excavated.

In strong rock that is not adversely impacted by major fault releases, achievable interramp slope angles are limited by the bench face angles that can be achieved. The bench face angle, the bench height, and the designed bench width to provide adequate rock fall protection define the interramp slope angle. Controlled blasting in the zone near the designed bench face will serve to limit damage to the rock mass and provide the steep bench faces required to achieve the recommended interramp slope angles.

Structural domains that contain intermediate to long faults that strike and dip adversely to the designed pit walls impact the interramp slope angles that can be achieved. When long members of these faults are undercut by interramp slopes, plane shear or wedge failures occur. These structures are identified and analyzed statistically to estimate the volume of interramp slope failures in defined pit sectors for various interramp slope angles.

Non-daylighted faults provide releases and boundaries to failures where weak rock mass between the toe of the slope and the release structures is not strong enough to support the stresses in the toe of the slope.

### **3.2 Faults Identified at the Castle Mountain Mining Property**

The main fault orientation mapped within the Castle Mountain Mining property is a NNE to NE striking dipping steeply to the SE. A few faults dip antithetically to the NW. Faults within this major system are sinuous and form “Y” shaped intersections with other faults of similar strike. Taylor (2015) reported that the fault pattern is typical of regional extension or collapsing of a caldera as the magma was evacuated from the magma chamber due to the intense volcanic activity. Evidence of the collapsing caldera included observations that faults in the lower strata of the caldera volcanics cannot be traced into upper units, indicating that faulting was contemporaneous with the period of volcanic activity associated with that phase of the volcanic cycle.

Figure 3-2 shows an equal area Schmidt plot of the fault structures greater than 60 feet long mapped by Capps in 1991 in the JSLA pit, and by CNI from cell mapping conducted in the JSLA pit in 1993 and in the Oro Belle pit in 2017. As shown, the main fault set dips greater than 60 degrees to the SE. The mean orientation of this fault set is expressed as a dip direction of 117 degrees and a dip of 75 degrees. This trend is also representative of the following geologic features: dominant joint orientation, alignment of rhyolite domes, trend of mineralization, and trend of major paleo-channels.

A few EW striking to WNW steeply dipping faults were mapped in the Miocene volcanic rocks. This structural trend has been reported as a major fabric in the Proterozoic basement rocks and is thought to have been reactivated during the regional extension associated with the Miocene volcanics.

EQX geologists have mapped the major faults throughout the project and Figure 3-3 shows the mapped faults draped on the preliminary pit design. Downhole drill data indicate that there are some intensely altered intervals that do not correspond to the major mapped faults. EQX geologists indicate that the lesser faulting has not been mapped.

### **3.3 Rock Fabric – Cell Mapping**

Minor discontinuities such as rock joints are termed rock fabric. Because of the highly variable nature of the length, spacing, and orientations of these discontinuities, statistical methods are used to characterize these parameters for the dominant joint sets. Rock fabric, including joints, bedding, and foliation, impact the bench face angles that can be achieved. The statistics for these structures are defined using a mapping method developed by CNI known as cell mapping.

Figure 3-4 shows a lower hemisphere plot of the joint and bedding joint mapped during the 1993 and 2017 cell mapping campaigns at the Castle Mountain property. Figure 3-5 shows the location of the cells mapped by CNI during these two campaigns. As shown in Figures 3-2 and 3-4, the dominant north to northeast striking joint set orientation matches the dominant fault set orientation. The WNW steeply dipping joint matches the Proterozoic fault set mentioned in the previous section of this report. The cell mapping data collected as part of the 1993 and 2017 cell mapping campaign is reported in *Appendix B - 1993 and 2017 CNI Cell Mapping*.

The major bedding orientation of tuffaceous strata dips to the WNW. Taylor (2015) reported that this bedding dip indicates that the strata were rotated to the west as fault bounded grabens formed during the collapse of the caldera. Some minor bedding dips to the SSE and SSW were mapped and may be related to local rotations bounded by smaller fault bounded grabens.

### **3.4 Rock Fabric – Televiewer Data**

Acoustic televiewer surveys can be used to obtain rock fabric information from boreholes where no surface exposure exists. CNI logged and analyzed four televiewer survey holes at Castle Mountain drilled specifically for the designed expansion phases: GT-001, GT-002, GT-003, and GT-004 (Figure 3-6). The locations, depths, and orientations of these drill holes were chosen to optimize coverage with respect to the final design, as well as to avoid any ‘blind zones’ that can occur when a drill hole does not intersect certain geologic features due to their orientations relative to the drill hole. Structures measured in the televiewer surveys are presented as stereonets by core hole in Figures 3-7 to 3-10, in all of the merged joints in Figure 3-11, in all of the merged faults in Figure 3-12, and by rock type in Figures 3-13 to 3-17. The

televiewer data collected during this core logging campaign is reported in *Appendix C - 2019 Televiewer Data*.

Analysis of the televiewer data for the four core holes reveals the following:

1. The dominant joint set centers around an average dip direction (DDR) of 104° and dip of 79°. Rhyolite and Epiclastic rocks exhibit the strongest representation of this set.
2. The dominant fault set is similar to the dominant joint set with an average DDR of 111° and dip of 84°, including opposite-dipping faults with an average DDR of 289° and dip of 88°. Another strong set with slightly lower dips has an average DDR of 136° and dip of 65°.
3. Low angle joints are most pronounced in Andesite with an average DDR of 132° and dip of 16°, Epiclastic rocks with a DDR of 76° and a dip of 25°, Rhyolite with a DDR of 274° and dip of 27°, and Volcaniclastics with dips ranging from 3° to 30°, and sets with average DDRs at 50°, 160°, and 260°.

### **3.4.1 Geomechanical Logging**

Core logging of the four drillholes consisted of collecting detailed geomechanical data for each drill hole. Geomechanical data is measured directly on the core to determine mechanical properties of the rock, including degree of fracturing, hardness, recovery, and other parameters.

The logged geomechanical data parameters included:

1. Drill interval (from and to depths)
2. Length of core recovered
3. Rock quality and fracture frequency
  - a. Length of longest core piece
  - b. Total length of core pieces greater than or equal to 0.4 foot (2 times the core diameter = rock quality designation [RQD])
  - c. Total length of core pieces greater than or equal to 1.0 and 1.5 feet
  - d. Number and length of whole pieces
  - e. Total length of broken core
  - f. Total length of rubble
  - g. Average hardness
  - h. Total length of core with a hardness less than or equal to R2
  - i. Number of joint sets (Jn)
  - j. Joint roughness (Jr), and alteration (Jn)

The RQD data are used in estimating the rock-mass shear strengths for analyzing interramp and overall slope stability. RQD, along with the joint properties data ( $J_r$  and  $J_a$ ), may also be used to estimate the Geological Strength Index (GSI) for each drill interval, which is a method of estimating rock-mass strength and is commonly used when communicating rock-mass strengths in regards to slopes (Hoek, et al., 2013):

$$GSI = 52 * \frac{\frac{J_r}{J_a}}{1 + \frac{J_r}{J_a}} + \frac{RQD}{2}$$

The geomechanical data collected during this core logging campaign is reported in *Appendix D - 2019 Geomechanical Data*. Downhole plots of RQD and GSI for each core hole are presented in Figure 3-18, along with down hole bar charts of core quality in Figure 3-19. Cumulative frequency RQD plots for each formation are shown in Figure 3-20. The average RQD and GSI for each formation within the core holes are shown in Table 3-1.

**Table 3-1. Average RQD and GSI Values by Rock Type**

| Rock Type            | Average RQD | Average GSI |
|----------------------|-------------|-------------|
| Andesite             | 64.5%       | 54.7        |
| Autoclastic          | 26.4%       | 34.4        |
| Epiclastic           | 46.9%       | 43.1        |
| Rhyolite Apheric     | 43.3%       | 45.7        |
| Rhyolite Porphyritic | 29.6%       | 36.6        |
| Volcaniclastic       | 35.3%       | 35.8        |

Geomechanical logging of the core from all four holes reveals the following:

1. Andesite consistently has the highest RQD and GSI values, with an overall average of 64.5% RQD and GSI of 54.7 (Andesite was not encountered in core hole GT-003).
2. Epiclastic rocks have an average RQD of 46.9% and GSI of 43.1, though the average is much lower in GT-002 (24.1% RQD and 27.6 GSI) than in GT-001 (57.5% RQD and GSI of 52.5) and GT-003 (54.5% RQD and GSI of 45.2) (Figure 3-18).
3. Volcaniclastics have an average RQD of 35.3% and GSI of 35.8, though significant variation exists between core holes. For example, GT-001 has an average Volcaniclastic RQD of 22.5% and GSI of 27.8, while GT-002 has an average Volcaniclastic RQD of 46.4% and GSI of 42.8 (Figure 3-18).
4. Rhyolite is partitioned into the apheritic and porphyritic varieties, with the apheritic rhyolite showing higher average RQD and GSI values at 43.4% and 45.7, and the porphyritic rhyolite showing average RQD and GSI values of 29.6% and 36.6.

5. Autoclastic rocks represent a relatively small portion of the analyzed core, though they may prove to be a significant geotechnical rock type because of their low average RQD of 26.5% and GSI of 34.4.

#### 4.0 LABORATORY TESTING AND ROCK-MASS STRENGTHS

The purpose of geotechnical laboratory testing is to determine intact rock and fracture-shear strengths, which are used to estimate rock-mass strengths used for the overall slope analyses. Rock-mass quality and structural anisotropies are used along with the laboratory strength testing to estimate the strength of the rock mass. To estimate rock-mass strengths, the intact and fracture shear strength data for the various rock types are determined, and the rock-mass strengths are calculated based on rock quality zones distinguished first by rock and alteration type, and then by statistically similar RQD values for the stability sections analyzed. All data used in the rock strength estimates are presented in *Appendix E - Rock Strength Data*.

Building upon the prefeasibility report completed in 2017, a full suite of laboratory tests was completed on the major rock units found within the project. A manifest of the completed laboratory tests is provided in Table 4-1.

**Table 4-1. Laboratory Testing Manifest**

| <b>Geology</b> | <b>Uniaxial</b> | <b>Triaxial</b> | <b>Brazilian</b> | <b>SSDS</b> |
|----------------|-----------------|-----------------|------------------|-------------|
| Volcaniclastic | 3               | 3               | 3                | 0           |
| Epiclastic     | 3               | 4               | 3                | 3           |
| Rhyolite       | 9               | 10              | 9                | 8           |
| Andesite       | 6               | 7               | 6                | 3           |

Small Scale Direct Shear (SSDS) samples of the volcaniclastic unit were difficult to collect due to the degraded nature of the material, and clean fractures were non-existent in the recovered core.

The CNI method to estimate rock-mass strengths uses the intact strength and the direct shear strength of the fractures to estimate the rock-mass shear strength. This method is explained in Section 4.5 “Rock-Mass Strengths.” The Hoek-Brown method for determining the rock-mass shear strength uses a rock-mass classification system and estimated intact triaxial shear strength parameters to estimate the rock-mass shear strength.

The multi-bench failures that occurred in mining the Jumbo North and the Oro Belle pits were related to weak clay altered rock and faults that acted as a back-plane weakness. Additional samples of the weak clay altered material were collected and tested to add to the database of clay strengths.

#### 4.1 Spatial Rock Quality

Attempts were made to spatially characterize the rock quality designation (RQD) within each of the geologic units (Rhyolite, Volcaniclastic, Epiclastic, and Andesite), but no substantial correlations could be made. Within each geologic unit, data were filtered to within 100, 200, and 500 feet of the major faults to see if the RQD changed or if any trends could be found. Using the 30<sup>th</sup> percentile value of the available RQD data in each spatial bin, the Epiclastic and Andesite units were found to be within 5% RQD of their overall dataset, as reported in Table 4-2. Based on engineering judgement, the 30<sup>th</sup> percentile RQD value of 37% was used to calculate rock-mass strengths for the Epiclastic and Andesite units, irrespective of location. The RQD data for the Epiclastic and Andesite units appear to be normally distributed and are presented in Figure 4-1.

Using the 30<sup>th</sup> percentile RQD value for each spatial bin described above, the Rhyolite and Volcaniclastic units had slightly greater than a 10% difference in RQD compared to the overall dataset as reported in Table 4-2. The Rhyolite trends to higher RQD data the further the measurements get from the faults, but the Volcaniclastic trends to lower RQD values the further the measurements are from the faults. Tabulated data showing the 30<sup>th</sup> percentile RQD values at different distances from major faults are presented in Table 4-2.

**Table 4-2. 30<sup>th</sup> Percentile RQD Values at Different Distances from Major Faults**

| <b>Distance (ft)</b> | <b>Rhyolite</b> | <b>Volcaniclastic</b> | <b>Epiclastic</b> | <b>Andesite</b> |
|----------------------|-----------------|-----------------------|-------------------|-----------------|
| 100                  | 11.0            | 32.9                  | 35.8              | 41.1            |
| 200                  | 17.1            | 26.4                  | 38.2              | 37.0            |
| 500                  | 19.0            | 24.2                  | 37.8              | 35.0            |
| All                  | 24.8            | 22.0                  | 37.0              | 37.0            |

|                       |             |             |            |            |
|-----------------------|-------------|-------------|------------|------------|
| <i>Max Difference</i> | <i>13.8</i> | <i>10.9</i> | <i>1.2</i> | <i>4.1</i> |
|-----------------------|-------------|-------------|------------|------------|

Due to the discrepancy of data for the Rhyolite and Volcaniclastic units, a different approach was taken to estimate rock quality for these units. A histogram of the available RQD show that the data appear to be more uniform in the RQD range from 0 to 60%, and tapers off at RQD values greater than 60% data, which then tapers off at the higher RQD values. The histogram showing this relationship is presented in Figure 4-2. A 30% RQD value was used to estimate the rock-mass strengths for the Volcaniclastic and Rhyolite units. The 30% RQD value

is the average RQD found within the uniform portion of the distribution for both the Volcaniclastic and Rhyolite units.

#### 4.2 **Fracture Shear Strength**

Slope displacements in open-pit mines typically occur along pre-existing geological discontinuities (natural fractures and faults), and at times through a combination of these structures and the rock mass. Consequently, determination of the shear strength of these joints and faults is an important input into the assessment of structural failures in the bench and interramp scale analyses. Additionally, the discontinuity strengths may be important to determine the strength of a defined anisotropy in the rock mass, or as a discrete back plane release that combines with a potential failure through the rock mass at the toe of the slope. The direct-shear test is used for measuring the shear strength along discontinuities. The test consists of applying a normal load to the discontinuity, which separates two blocks of rock. A shear load is then applied to displace the blocks relative to one another.

Table 4-3 reports the fracture shear strength used for the various rock strength categories defined at Castle Mountain. These strengths range from clay fillings to clean fractures and probably are slightly conservative for the stronger rocks. Because no fracture samples of the Volcaniclastic unit could be collected from the 2019 geotechnical drilling campaign, the Epiclastic friction angle and cohesion were used as a substitute for the analyses.

**Table 4-3. Fracture Shear Strengths**

| <b>Lithology</b> | <b>Friction Angle (deg)</b> | <b>Cohesion (psi)</b> |
|------------------|-----------------------------|-----------------------|
| Andesite         | 22.8                        | 7.6                   |
| Rhyolite         | 31.6                        | 11.2                  |
| Epiclastic       | 24.2                        | 15.0                  |

The following equation defines the linear shear-strength:

$$\tau = \sigma_n (\tan \phi) + C$$

where:

$\tau$  = Shear Stress  
 $\sigma_n$  = Normal Stress  
 $\phi$  = Friction Angle  
 $C$  = Cohesion

### **4.3 Weak Clay-Altered Material Strength**

As identified in the 2017 geotechnical prefeasibility study, there is a weak clay-altered material that is associated with most of the instabilities that occurred during the previous mining. These weak clay-altered units are generally found in proximity with the major faults identified by EQX geologists, as well as other minor faults that have been intersected with geotechnical drilling. The minor faults are not extensively modeled and therefore cannot be considered in geotechnical analysis at this time.

Laboratory tests were conducted on clay-altered material collected during the 2019 geotechnical drilling campaign. The samples exhibited a wide variability in strengths compared to the remold testing conducted in 2017. Three back analyses have also been conducted on previous failures to calibrate the weak clay-altered strengths. Figure 4-3 shows 1) the laboratory tested residual shear strength by sample, and 2) the back-analyzed Mohr-Coulomb strengths determined in the three historical failures, where failure occurred through a weak altered rock mass. All of the tested samples were weaker than the back analyzed strengths, which indicates that the sampling of this material for testing was biased toward the weakest materials collected on the surface exposures in 2017 and in the core in 2019.

Therefore, for the stability analyses performed for the present study, the residual clay strengths tested in 2017 were used for the weak altered material surrounding the major named faults at the Castle Mountain Project. The 2017 clay strengths are more consistent in friction angle and cohesion and are slightly more conservative than the back-analyzed clay strengths. The 2017 residual direct shear tests for samples OCM-OB-02 and OCM-OB-04 were combined to provide the shear strength defined as a friction angle of 18.8 degrees and a cohesion of 14.9 psi.

#### **4.3.1 *Remolded Direct Shear Tests on Clay Samples***

Two strongly clay-altered samples were collected in the Oro Belle pit for the 2017 study to determine the residual shear strength of this weak material. The samples (OCM-OB-02 and OCM-OB-04) were collected in the NW and SW walls of the Oro Belle pit, respectively. Sieve analyses, Atterberg limits tests, XRD analyses, and direct shear tests were performed to characterize these weak materials. The Atterberg limit tests are conducted on the material that is finer than 40 mesh (0.425 mm), which includes the fine sand to silt and clay sizes. These limits

determine the moisture contents at which the samples are in a plastic and liquid state. This test is used to determine how plastic the sample acts as defined by the plasticity index (the difference between the moisture content at the liquid limit and the moisture content at the plastic limit). A sand has no plasticity and a clay can hold a significant range of moisture in the plastic range. Mesri (2003) correlated the plasticity index to the shear strength of soils with significant volumes of clay. This correlation is instructive, but samples that have appreciable coarser grains (sand to gravel size) will increase the shear strength of clayey soils. Figures 4-1 and 4-2 report the sieve analyses and Atterberg limit results for samples OCM-OB-02 and OCM-OB-04.

The XRD analyses performed by DCM Science Laboratory in Wheat Ridge, Colorado are attached to this report as *Appendix F - X-Ray Diffraction Results*. Sample CM-OB-02 was 41% quartz and 59% rectorite, a one to one regular interstratification of muscovite/illite and smectite. CM-OB-04 was 23% quartz, 24% calcite, and 47% mixed layer illite/smectite (85% smectite).

In addition to the two surface samples, five clay samples were collected from the 2019 geotechnical drilling for testing. Table 4-4 summarizes the remolded direct shear tests with the best fit residual shear strength for each of the samples.

**Table 4-4. Remolded Clay Direct Shear Strengths**

| <b>Drill Hole</b> | <b>Sample</b>        | <b>Friction Angle (deg)</b> | <b>Cohesion (psi)</b> |
|-------------------|----------------------|-----------------------------|-----------------------|
| GT001             | 19648-CMM-GT001-0685 | 2.5                         | 8.0                   |
| GT002             | 19648-CMM-GT002-0403 | 24.6                        | 8.4                   |
| GT002             | 19648-CMM-GT002-0429 | 13.9                        | 13.7                  |
| GT003             | 19648-CMM-GT003-0575 | 9.9                         | 12.7                  |
| GT004             | 19648-CMM-GT004-0965 | 9.1                         | 7.3                   |
| Surface           | 17515-CM-OB-02       | 18.4                        | 16.4                  |
| Surface           | 17515-CM-OB-04       | 19.3                        | 13.3                  |

#### **4.3.2 Back-Analyzed Clay Strengths**

Clay strengths were obtained by back-analyzing three historical failures in the Oro Belle and Jumbo North pits. The density of the materials analyzed was estimated to be 135 pcf. Using the Oro Belle Upper East Wall, Jumbo North Wall, and Oro Belle West Wall failure geometries, a relationship was developed between the friction angle and cohesion at a Factor of Safety just

below 1.00. This relationship, along with the laboratory tested residual shear strengths of remolded clay samples, is shown in Figure 4-3.

### ***Oro Belle Upper East Wall***

The first back analysis was performed on the upper eastern wall of the Oro Belle pit. The original plan indicated a slope height of 260 feet and slope angle of roughly 52 degrees, but was eventually laid back to 33 degrees to mitigate the failure. The pre-failure geometry was analyzed at friction angles of 18.8 degrees, 22 degrees, and 26 degrees. Cohesions for each friction angle were determined that yielded factors of safety slightly less than 1.00. The pairs of friction angle and cohesion that resulted in a FOS of slightly less than 1.00 are plotted on Figure 4-3.

### ***Jumbo Northwest Wall***

The second back analysis was performed on a slope failure that occurred just below the haul ramp on the northwest wall of the Oro Belle pit. The as-built topography shows an overall slope height of 120 feet with a slope angle of 49 degrees. The pre-failure geometry was analyzed at friction angles of 18.8 degrees, 22 degrees, and 26 degrees. Cohesions for each friction angle were determined that yielded factors of safety slightly less than 1.00. The pairs of friction angle and cohesion that resulted in a FOS of slightly less than 1.00 are plotted on Figure 4-3.

### ***Oro Belle West Wall***

The third back analysis was performed on a slope failure that occurred on the west wall of the Oro Belle pit. The area had previous instabilities in the upper portion of the wall at some point between the original mining and 2017, when the geotechnical prefeasibility study was conducted. Between 2017 and 2020, the lower portion of the slope failed within this fault zone. The pre-failure topography shows an overall slope height of 450 feet with a slope angle of 45 degrees. The pre-failure geometry was analyzed at friction angles of 18.8 degrees, 22 degrees, and 26 degrees. Cohesions for each friction angle were determined that yielded factors of safety slightly less than 1.00. The pairs of friction angle and cohesion that resulted in a FOS of slightly less than 1.00 are plotted on Figure 4-3.

#### 4.4 Intact Rock Strength Testing

The intact shear strength of rock can be estimated from uniaxial compression, point load, Brazilian disk tension, and triaxial compression tests. Laboratory tests were conducted on samples from the 2019 drilling campaign to fill in the gaps of the intact rock strength estimates that were lacking in the original 2017 prefeasibility study.

##### 4.4.1 *Intact Shear Strength Based on Uniaxial Compressive Strength and Tensile Strength*

The intact rock shear strength can be estimated if the uniaxial compressive strength (UCS) and the tensile strength (TS) of the rock are known. Table 4-5 shows the average compressive strength and the average tensile strength for each of the geologic units, and the resulting intact friction angle and cohesion resulting from these averages. The Volcaniclastic and Epiclastic laboratory tests were combined due to similar uniaxial, triaxial, and disk tension results.

**Table 4-5. Intact Strength Summary**

| <b>Lithology</b>          | <b>UCS (psi)</b> | <b>TS (psi)</b> | <b>Friction Angle (deg)</b> | <b>Cohesion (psi)</b> | <b>Density (pcf)</b> |
|---------------------------|------------------|-----------------|-----------------------------|-----------------------|----------------------|
| Andesite                  | 7466             | 643             | 48.7                        | 1073.2                | 146.1                |
| Rhyolite                  | 18000            | 1419            | 49.8                        | 2476.8                | 142.8                |
| Volcaniclastic/Epiclastic | 5612             | 730             | 42.8                        | 991.7                 | 139.2                |

These results are derived from the transformation of the stresses from principal stress space to normal and shear stress space, according to Obert and Duvall (1967):

$$\phi_{intact} = \tan^{-1} \left( \frac{\beta - 1}{2\sqrt{\beta}} \right)$$

$$C_{intact} = \left( \frac{\sigma_c}{2\sqrt{\beta}} \right)$$

where:

$\sigma_c$  = Uniaxial Compression Strength (Y axis intercept in  $\sigma_1/\sigma_3$  space)

$\sigma_t$  = Tensile Strength

$$\beta = \frac{\sigma_c}{\sigma_t}$$

Additionally, values in Table 4-5 were corrected based on an empirical relationship developed by CNI between these intact linear strength estimates and linear fits to triaxial compression data. The corrections are as follows:

$$\phi_{i-estimated} = 0.85 * \phi_{empirical}$$

$$C_{i-estimated} = 0.98 * C_{empirical}$$

#### **4.5 Rock-Mass Strengths**

Overall slope failures can result from 1) daylighting large weak structures such as faults, bedding planes or lithologic contacts, 2) shearing stresses that exceed the strength of the rock mass, and 3) pore water pressure. An overall slope failure may occur as a combination of the factors listed above. For example, large slope failures typically have a structural anisotropy that may or may not daylight. The rock mass between the toe of the slope and a non-daylighted anisotropy and/or weak fault may fail if the stresses in the rock mass between the anisotropy and the toe of the slope exceed the rock-mass strength. To analyze the overall stability of a slope, the rock-mass strength must be estimated for zones identified as having statistically distinct strength characteristics.

The rock-mass shear strength is a function of the following:

1. Intact block size (related to RQD, fracture frequency, and number of joint sets)
2. Intact-rock shear strength
3. Fracture shear strength
4. Fracture orientations

Rock-mass strength estimates are based on characterizing the rock mass according to the parameters above. CNI developed a method to estimate the rock-mass strength that has been used successfully for more than 25 years for large open-pit design. The CNI approach was described on pages 130-132 in the published summary of the Large Open Pit (LOP) project entitled *Guidelines for Open Pit Slope Design*. An additional explanation of the method was published in Chapter 4 of a compilation of papers related to open pit slope stability titled *Slope Stability in Surface Mining*. The CNI method is described in section 4.5.1 of this report (“CNI Rock-Mass Strength Estimation Method”).

The Hoek-Brown (1980, 1988) rock-mass strength estimation method is commonly used by geotechnical practitioners. This method has undergone numerous modifications based on its

use to back analyze failures and in forward analyses of slope stability and underground stability studies. In 1994 through 1997, Hoek, et.al., published papers relating the rock-mass strength parameters used in the method to a rock mass classification system called the Geological Strength Index (GSI). Originally, the GSI was estimated from Bieniawski's RMR classification system. In the 1989 version of the RMR system, the GSI was estimated as the RMR value with the ground water rating set to 15 and the joint orientation adjustment set to 0. Today, the method uses a classification matrix to estimate the GSI. The matrix currently used for the GSI classification is shown as Table 5.34 on page 126 in the published summary of the Large Open Pit (LOP) project titled *Guidelines for Open Pit Slope Design*. The Hoek-Brown method is also described in detail on pages 123-130 in the LOP publication. Figure 4-4 shows the GSI rock-mass classification matrix.

#### 4.5.1 CNI Rock-Mass Strength Estimation Method

The rock-mass shear strength cannot exceed the intact-rock strength nor can it be less than the fracture shear strength. Intact-rock strengths must be reduced depending on the degree of fracturing. Experience with back-analyses of failures, as well as with fracture-modeling studies, indicates that the strength of the rock mass is a function of the ratio between the rock mass and rock substance (intact) elastic moduli.

More specifically, the relationship between the intact-rock and the rock-mass strength is proportional to the square of the modulus ratio. The rock-mass strength is determined as follows:

$$\begin{aligned}\tan \phi_{mass} &= \tan \phi_{intact} r_{\phi}^2 + \tan \phi_{fracture} (1 - r_{\phi}^2) \\ C_{mass} &= C_{intact} r_c^2 + C_{fracture} (1 - r_c^2)\end{aligned}$$

where  $r$  is  $<1$  and is equal to the modulus ratio:

$$r = \frac{E_{mass}}{E_{lab}}$$

and where  $E$  is equal to Young's Modulus.

Modified from Bieniawski (1978), the following illustrates the empirical relationship between RQD and the modulus ratio:

$$r_c = \frac{E_{mass}}{E_{lab}} = 0.225e^{0.013 * RQD}$$

and

$$r_{\phi} = \frac{E_{mass}}{E_{lab}} = 0.3775e^{0.0075*RQD}$$

where RQD is expressed as a percentage.

The modulus ratio related to the rock-mass friction angle ( $r_{\phi}$ ) was modified to more accurately describe the friction angles derived in back-analyses of slope failures. Bieniawski's original ratio definition yielded friction angles that over-estimated the rock mass friction angle according to the back analyzed failures. The rock-mass strength estimates used in the slope stability analyses for this study are presented in Table 4-6.

**Table 4-6. Rock-Mass Strength Estimates**

| <b>Lithology</b> | <b>Friction Angle (deg)</b> | <b>Cohesion (psi)</b> | <b>Density (pcf)</b> | <b>RQD</b> | <b>CRF</b> |
|------------------|-----------------------------|-----------------------|----------------------|------------|------------|
| Andesite         | 30.9                        | 74.4                  | 146.1                | 37         | 0.50       |
| Rhyolite         | 36.6                        | 99.2                  | 142.8                | 30         | 0.35       |
| Volcaniclastic   | 29.1                        | 61.4                  | 139.2                | 30         | 0.50       |
| Epiclastic       | 29.6                        | 72.2                  | 139.2                | 37         | 0.50       |

#### **4.5.2 Comparison of CNI and Hoek-Brown Rock-Mass Strength Estimation Methods**

Based on experience, CNI has utilized correlations between measured joint strength from the laboratory and the RQD rock quality parameter to estimate GSI. The correlation matrix shown in Figure 4-4 explains the method used to estimate GSI from RQD and fracture shear strength.

The CNI method is a post-peak rock-mass strength estimation that uses measurable data. Figures 4-5 shows a comparison between the CNI rock-mass strength estimation and the Hoek-Brown rock-mass strength estimation for the Rhyolite material. The Hoek-Brown estimate of rock-mass strength assumed a disturbance factor of 0.7, which indicates reasonable care in blasting.

## 5.0 BENCH DESIGN

In pit slope sectors where the rock quality and major structure orientations are favorable, the bench design is the control on the interramp slope angles that can be achieved. The rock fabric, blast damage, and excavation practices impact the bench face angles that can be achieved. The bench face angle, along with the bench width required for rock fall protection, dictate the interramp slope angle that can be achieved. Several studies have been conducted to determine bench widths required to contain rockfall, most notably those published by Ritchie (1963) and the Oregon Department of Transportation (ODOT, 2001).

Recent research at CNI was conducted to estimate ranges of blast damage required to obtain measured bench face angles relative to the joint characteristics measured in discrete structural cells mapped in bench face exposures. Field observations of bench faces indicate that back break occurs along joint sets that form day-lighted plane shear and wedge geometries. When the joint orientation that controls the back break is determined, the number of mean joint spaces required to geometrically form the measured bench face angle are determined. The number of spaces that are required for the blasting to break to arrive at the measured bench face angle is a function of the mean joint spacing, the maximum length observed for the joint set, and the angle that the strike of the joint makes with the strike of the bench face. Although the mean joint spacing correlates reasonably well with the number of joint spaces that must be broken to calibrate to the measured bench face angle, the correlation becomes significantly better when the mean spacing is multiplied by the longest joint observed and the angle to the bench face strike, as explained below.

Figure 5-1 shows the broken spaces needed to obtain the measured bench face angle for the southwest walls mapped in the JSLA pit in 1993 and the Oro Belle pit in 2017 as a function of mean joint spacing. The data is fit best with a logarithmic function. Figure 5-2 shows the same dataset plotted on a log-log plot. A better fit to the data is had when the angle of the control structure to the bench face strike and the length of that structure are multiplied to the spacing, as shown in Figure 5-3.

It is postulated that a significant proportion of the remaining variance in the model shown in Figure 5-3 is related to blast damage. When more spaces are broken in the blasting process, the effective bench face angles are reduced. Figure 5-4 illustrates the definition of the effective

bench face angle (the angle between the toe of the bench and the crest of a viable rock containment bench). Figure 5-5 shows the blast damage plot at a mine that was experimenting with pre-split blasting to obtain steeper bench face angle. Cells were mapped in the same pit sector where pre-splits and no pre-splits were used in the blast patterns. The two sets of data indicate that the “no” pre-split benches suffered more breakage.

### **5.1 Example of Estimating Bench Face Angle in SW Wall of Castle Mountain Pits**

The blast damage curve for the southwest wall, with a slope direction of 45 degrees, is shown in Figure 5-6. The equation for the mean damage curve to arrive at the measured bench face angles is also shown in the figure. If excellent blasting is practiced, the y intercept of the log-log plot is reduced from 2.60 for the mean curve to 2.35.

To smooth out the estimated bench face angle curves, the length, spacing, and orientation of the joint sets that control the back break are statistically sampled. The lengths and spacing are sampled according to a log normal distribution (Priest and Hudson, 1981). The joint orientations are sampled by randomizing the trend and plunge vector representing the pole of the joint according to the normal distribution. Sampling of the pole of the joint within one standard deviation of the mean gave reasonable results. The sampled poles reside within a cone of roughly 10 to 15 degrees from the mean pole.

For each sampled orientation (spacing and length), the back break is estimated by using the blast damage model shown in Figure 5-6 to estimate the number of spaces that break to fit the model. A geometric calculation can then be made to estimate the back break caused by the controlling joint set. Figure 5-7 shows the modeled bench face angles as a cumulative distribution curve. The curves shown include 1) a theoretical curve, which is the distribution if only one structure within the joint set fails out of the bench, 2) a predicted curve for average controlled blasting that was carried out during the previous mining, and 3) a predicted curve for a slight improvement in controlled blasting procedures.

For design purposes, the bench face angle estimates from the slightly improved controlled blasting predicted curve were used for the current recommendations for pit sectors, where bench design controls the interramp slope angle recommendation. The cumulative distribution curves of theoretical and predicted bench face angles for other expected major slope orientations are presented in *Appendix G - Modeled Bench Face Angle Curves*.

For design purposes, CNI uses the 80% reliable bench face angle (20% of the modeled bench faces are less than this value). As discussed in the next section, this BFA, along with a minimum catch bench width required to contain rock fall, dictates the interramp slope angle. The theoretical, regular blasting, and improved blasting bench face angles for 80% reliable benches are plotted as a function of slope dip direction in Figure 5-8.

## 5.2 Catch-Bench Width

CNI uses the Modified Ritchie Criterion as a guide for designing catch-bench widths. This method evolved following publication of a technical paper by A. M. Ritchie in 1963 on the design of highway shoulders for catching rockfall originating from excavated and natural slopes. Ritchie's investigation was limited to a relatively small number of slope angle and slope height geometries and therefore requires extrapolation for use in open-pit mining. Because slope (bench) height is one of the most important controls on the distance a rock will travel when detached from the bench, Richard Call suggested the empirical relationship between the slope height and average, or preferred, catch-bench width based on his experience:

### **Modified Ritchie Criterion (MRC) for Catch-Bench Width**

$$\text{Catch-bench width (feet)} = 0.2 * \text{bench height} + 15 \text{ feet}$$

so, for single, double, and triple benching:

$$\text{(Single-bench width) } 19 \text{ feet} = 0.2 * 20 \text{ feet} + 15 \text{ feet}$$

$$\text{(Double-bench width) } 23 \text{ feet} = 0.2 * 40 \text{ feet} + 15 \text{ feet}$$

$$\text{(Triple-bench width) } 27 \text{ feet} = 0.2 * 60 \text{ feet} + 15 \text{ feet}$$

This equation is published in the SME Surface Mining Handbook (2nd edition, 1990, p875). CNI sponsored research at the University of Arizona in 1987 in which it demonstrated the use of this criterion in benched mine slopes. In those field tests, the MRC was found to be conservative for containing rockfall in a limestone slope benched on 40- to 50-foot heights. At a height of 100 feet, the catch-bench width was more marginal in controlling rockfall. The MRC serves as a good general guide with wide applicability.

### 5.3 Catch-Bench Design

For bench-scale design, the maximum achievable ISA depends on the BFA that corresponds to the desired reliability for the design bench height. The design requirement of 80% reliability for benches means benches must achieve MRC width 80% of the time. Figure 5-9 shows the predicted bench face angle distribution for the SW slopes and the bench face angle associated with an 80% reliability that the bench faces will be greater than this value.

The 80% reliable BFA and the MRC catch bench width are used to calculate the recommended interramp slope angle. However, when the benches are constructed, the trim or pre-split shots are drilled near vertical (80 to 90 degrees from horizontal), so most catch bench widths are wider than the MRC catch bench width. The recommended interramp slope design is calculated using the 80% reliability bench face angle and the MRC bench width; however, the design bench face angle and bench width are calculated using the median bench face angle.

The achievable ISA given a BFA is calculated using the following equation:

#### **Recommended ISA**

$$ISA = \tan^{-1} \left( \frac{BH}{CBW + BH * \frac{1}{\tan(BFA)}} \right)$$

where:

BH = Bench Height

ISA = Interramp Slope Angle

CBW = Catch-Bench Width (Modified Ritchie Criterion)

BFA = Bench-Face Angle, (80% reliability)

Based on experience, an additional 4- to 6-foot offset is included in the CBW for ISA calculations between each mining increment when a multi-increment bench height is designed. This additional distance is used to reflect horizontal offset required by drilling space issues between mining increments. Pre-splitting over the entire 60-foot triple bench increment will eliminate this offset. The recommended angles in this report assume that pre-splitting will be used and that the pre-split holes will be drilled in a single pass of 60 feet. This 60-foot height assumes a triple bench for a 20-foot mining increment.

Recommended interramp slope angles based on the bench scale analyses are listed in Table 5-1. However, overall analyses dictate the interramp angle that can be achieved in many of these wall orientations, especially in proximity to the major named faults.

**Table 5-1. Bench Scale Analysis Results**

| <b>Slope Dip Direction (degrees)</b> | <b>60-Foot-High Bench (MRC Width = 27 feet)</b> |                             |                                   |                                  |
|--------------------------------------|---|-----------------------------|-----------------------------------|----------------------------------|
|                                      | <b>Interramp Slope Angle (degrees)</b>          | <b>Design BFA (degrees)</b> | <b>80% Reliable BFA (degrees)</b> | <b>Design Bench Width (feet)</b> |
| 130 - 140                            | 50  | 80                          | 69                                | 39                               |
| 225 - 240                            | 56  | 80                          | 77                                | 30                               |
| 315 – 320                            | 55  | 80                          | 76                                | 31                               |
| 45                                   | 50  | 80                          | 69                                | 39                               |

## **6.0 OVERALL SLOPE ANALYSIS**

Stress levels in pit slopes can locally exceed rock-mass strengths. The strength of the rock mass must be evaluated and compared to the predicted stresses based on geotechnical, geological, and geomechanical parameters.

Two-dimensional limit-equilibrium overall slope analyses were performed using Rocscience's Slide 2018 software. Spencer's method of slices was utilized to calculate FOS values. A linear Mohr-Coulomb shear strength relationship was assumed for all rock types. A phreatic water surface and pore water pressure conditions were not evaluated for these analyses, as EQX indicated that the pit would be dry. A factor of safety is calculated from the ratio of the resisting forces and driving forces for multiple potential failure surfaces. The lowest FOS obtained from the potential failure surfaces is then optimized and assigned to the cross section. A FOS of 1.20 was selected as the design criterion for the as-designed and optimized slope designs.

Fifteen representative cross sections were selected for analysis on the preliminary pit designs provided by John Nilsson. Figure 6-1 shows the plan view location of fifteen analysis sections as related to exposed geology. Factors affecting the selection of the overall slope analysis sections included:

- Slope height and slope angle
- Potential for low rock-mass strength at the toe of the slope
- Location and orientation of potential weak fault zones
- Critical infrastructure placement at the crest of the pits

### **6.1 Model Input Parameters**

#### **6.1.1 *Geology Model***

EQX provided CNI with a three-dimensional geology model that was substantially different from the original model received in 2017. The individual geologic units were grouped together based on expected geomechanical rock quality.

### **6.1.2 *Material Properties***

The rock-mass strength parameters used for each section are discussed in Chapter 4, “Laboratory Testing and Rock-Mass Strengths.” Generic rock-mass strengths were created for each geologic unit and applied globally. Zones extending perpendicular from the major named faults were modeled using the weak altered strengths discussed in Chapter 4.

### **6.1.3 *Hydrogeology***

EQX personnel indicated that there was no water down to the final depths of the proposed pits. As a result, the recommended slope angles are based on dry conditions.

Water pressures play a crucial role when analyzing overall slope stability since water pressure reduces the effective normal stress on the shear plane. It should be noted that any pore water pressure will significantly impact slope stability. CNI recommends validating the groundwater conditions.

## **6.2 Results**

The overall results for the fifteen cross sections are presented in Table 6-1. The cross sections for each stability analysis are presented in Figures 6-2 through 6-30 with critical slip surfaces and the resulting FOS. All optimized slopes meet or exceed a 1.20 FOS except for Section 8. The 1.16 FOS that was calculated was due to the re-introduction of a large fault zone that was cut in the provided design. The final pit geometry will need to be evaluated for stability.

**Table 6-1. Overall Stability Analyses Results**

| Section | FOS         |           | Optimized ISA (deg) |          |            |                 |                    |                    |
|---------|-------------|-----------|---------------------|----------|------------|-----------------|--------------------|--------------------|
|         | As-Designed | Optimized | Rhyolite            | Andesite | Epiclastic | Volcaniclastics | ±100 ft from fault | ±200 ft from fault |
| 1       | 1.34        | 1.25      | 51                  | -        | -          | 50              | -                  | -                  |
| 2       | 1.56        | 1.21      | -                   | 48       | 50         | 50              | -                  | -                  |
| 3       | 1.32        | 1.22      | 51                  | -        | -          | 50              | -                  | -                  |
| 4       | 1.51        | 1.34      | 51                  | -        | -          | 50              | -                  | -                  |
| 5       | 1.35        | 1.35      | 51                  | -        | -          | -               | 40                 | -                  |
| 6       | 1.59        | 1.25      | -                   | 48       | 50         | 50              | -                  | -                  |
| 7       | 1.05        | 1.21      | 51                  | -        | -          | -               | -                  | 46                 |
| 8       | 1.51        | 1.16      | -                   | 48       | 50         | 50              | -                  | 40                 |
| 9       | 1.72        | 1.46      | 52                  | -        | -          | -               | -                  | -                  |
| 10      | 1.61        | 1.58      | 52                  | -        | -          | -               | -                  | -                  |
| 11      | 1.75        | 1.48      | 51                  | -        | -          | -               | -                  | -                  |
| 12      | 0.91        |           | -                   | -        | -          | -               | -                  | -                  |
| 13      | 1.51        | 1.28      | 52                  | -        | -          | -               | -                  | -                  |
| 14      | 1.52        | 1.34      | 51                  | -        | 50         | 50              | -                  | -                  |
| 15      | 1.62        | 1.33      | -                   | -        | 51         | 51              | -                  | -                  |

### 6.2.1 Section 1

Section 1 is located on the western side of the South Extension pit. The cross section has a total height of approximately 1010 feet, a slope dip direction of approximately 90 degrees, and an overall slope angle of 46 degrees. Major rock units present in the model include the Volcaniclastic, Epiclastic, and Rhyolite units. The critical slip surface on the provided pit design occurs throughout the overall slope with a FOS of 1.34. Changing the ISA within the Rhyolite to 51 degrees and within the Volcaniclastic to 50 degrees, results in a FOS of 1.25.

### 6.2.2 Section 2

Section 2 is located on the northwestern side of the South Extension pit. The cross section has a total wall height of approximately 1020 feet, a slope dip direction of approximately 140 degrees, and an overall slope angle of 42 degrees. Major rock units present in the model include the Volcaniclastic, Epiclastic, Rhyolite, and Andesite units. The critical slip surface on the provided pit design occurs throughout the overall slope with a FOS of 1.56. Changing the ISA within the Epiclastic and Volcaniclastic slopes to 50 degrees, and within the Andesite to 48

degrees, results in a FOS of 1.21.

### **6.2.3 Section 3**

Section 3 is located on the northwestern side of the South Extension pit. The cross section has a total wall height of approximately 1100 feet, a slope dip direction of approximately 120 degrees, and an overall slope angle of 47 degrees. Major rock units present in the model include the Volcaniclastic, Epiclastic, and Rhyolite units. The critical slip surface on the provided pit design occurs throughout the overall slope with a FOS of 1.32. Changing the ISA within the Rhyolite to 51 degrees and within the Volcaniclastic slopes to 50 degrees, results in a FOS of 1.22.

Section 3 is also the analysis where CNI calculated the 300-foot crest offset for critical infrastructure. An anisotropic strength was used where the fault strength would be applied to slices where the dip was between -90 to -65 degrees. This allows the fault to effectively move spatially and simulates the minimum offset distance required to maintain a 1.20 FOS. Using these assumptions, the maximum slip surface where the FOS is 1.20 was found at 282 feet behind the crest.

### **6.2.4 Section 4**

Section 4 is located on the southwestern side of the JSLA pit. The cross section has a total wall height of approximately 800 feet, a slope dip direction of approximately 50 degrees, and an overall slope angle of 44 degrees. Major rock units present in the model include the Volcaniclastic, Epiclastic, and Rhyolite units. The critical slip surface on the provided pit design occurs throughout the overall slope with a FOS of 1.51. Changing the ISA within the Rhyolite to 51 degrees and within the Volcaniclastic slopes to 50 degrees, results in a FOS of 1.34.

### **6.2.5 Section 5**

Section 5 is located on the eastern side of the South Extension pit. The cross section has a total wall height of approximately 1020 feet, a slope dip direction of approximately 270 degrees, and an overall slope angle of 39 degrees. Major rock units present in the model include the Volcaniclastic, Epiclastic, Rhyolite, Andesite, and fault zone units. The critical slip surface on the provided pit design occurs throughout the overall slope with a FOS of 1.35. For design purposes, the ISA of the Rhyolite was changed to 51 degrees, and a fault zone ISA of 40 degrees

was applied to a zone  $\pm 100$  feet from the modeled Dillon fault. Changing the ISA to meet these parameters yields the same 1.35 FOS.

#### **6.2.6 Section 6**

Section 6 is located on the north side of the South Extension pit. The cross section has a total wall height of approximately 1015 feet, a slope dip direction of approximately 190 degrees, and an overall slope angle of 37 degrees. Major rock units present in the model include the Volcaniclastic, Epiclastic, and Andesite units. The critical slip surface on the provided pit design occurs throughout the overall slope with a FOS of 1.59. Changing the ISA within the Andesite to 48 degrees and within the Volcaniclastic and Epiclastic slopes to 50 degrees, results in a FOS of 1.25.

#### **6.2.7 Section 7**

Section 7 is located on the southwestern side of the JSLA pit. The cross section has a total wall height of approximately 780 feet, a slope dip direction of approximately 45 degrees, and an overall slope angle of 44 degrees. Major rock units present in the model include the Volcaniclastic, Epiclastic, Rhyolite, and fault zone units. The critical slip surface on the provided pit design occurs throughout the overall slope with a FOS of 1.05. Changing the ISA within the Rhyolite to 51 degrees and applying an ISA of 46 degrees to a zone  $\pm 200$  feet from the modeled Maverick fault, results in a FOS of 1.21.

#### **6.2.8 Section 8**

Section 8 is located on the northwestern side of the JSLA pit. The cross section has a total wall height of approximately 960 feet, a slope dip direction of approximately 146 degrees, and an overall slope angle of 32 degrees. Major rock units present in the model include the Volcaniclastic, Epiclastic, Andesite, and fault zone units. The critical slip surface on the provided pit design occurs throughout the overall slope with a FOS of 1.51. Changing the ISA within the Andesite to 48 degrees and within the Volcaniclastic and Epiclastic slopes to 50 degrees, and applying an ISA of 40 degrees to a zone  $\pm 200$  feet from the modeled McLane fault, results in a FOS of 1.16. The significant difference in FOS is due to the removal of a haul road in the original design and exposure of a large fault zone.

### **6.2.9 Section 9**

Section 9 is located on the eastern side of the JSLA pit. The cross section has a total wall height of approximately 955 feet, a slope dip direction of approximately 270 degrees, and an overall slope angle of 42 degrees. Major rock units present in the model include the Volcaniclastic and Rhyolite units. The critical slip surface on the provided pit design occurs throughout the overall slope with a FOS of 1.72. Changing the ISA within the Rhyolite to 52 degrees and within the Volcaniclastic slopes to 52 degrees, results in a FOS of 1.46.

### **6.2.10 Section 10**

Section 10 is located on the eastern side of the East Ridge pit. The cross section has a total wall height of approximately 1010 feet, a slope dip direction of approximately 298 degrees, and an overall slope angle of 53 degrees. Major rock units present in the model include the Rhyolite unit. The critical slip surface on the provided pit design occurs throughout the overall slope with a FOS of 1.61. Changing the ISA within the Rhyolite to 52 degrees results in a FOS of 1.58.

### **6.2.11 Section 11**

Section 11 is located on the north side of the Jumbo pit. The cross section has a total wall height of approximately 800 feet, a slope dip direction of approximately 180 degrees, and an overall slope angle of 35 degrees. Major rock units present in the model include the Volcaniclastic, Epiclastic, and Rhyolite units. The critical slip surface on the provided pit design occurs throughout the overall slope with a FOS of 1.75. Changing the ISA within the Rhyolite to 51 degrees results in a FOS of 1.48.

### **6.2.12 Section 12**

Section 12 is located on the west side of the East Ridge pit. The cross section has a total wall height of approximately 510 feet, a slope dip direction of approximately 90 degrees, and an overall slope angle of 39 degrees. Major rock units present in the model include the Volcaniclastic, Rhyolite, and fault zone units. The critical slip surface on the provided pit design occurs throughout the overall slope with a FOS of 0.91. Due to the extensive nature of the fault zones, any remediation design would likely remove the entire slope. CNI recommends removing

this “island” found between the East Ridge and Jumbo pits, or understanding that leaving the “island” in will likely result in remediation work at a later date.

### **6.2.13 Section 13**

Section 13 is located on the eastern side of the Oro Belle pit. The cross section has a total wall height of approximately 1140 feet, a slope dip direction of approximately 270 degrees, and an overall slope angle of 45 degrees. Major rock units present in the model include the Rhyolite unit with small pieces of all other units. The critical slip surface on the provided pit design occurs throughout the overall slope with a FOS of 1.51. Changing the ISA for the overall slope to 52 results in a FOS of 1.28.

### **6.2.14 Section 14**

Section 14 is located on the northwestern side of Oro Belle pit. The cross section has a total wall height of approximately 990 feet, a slope dip direction of approximately 138 degrees, and an overall slope angle of 45 degrees. Major rock units present in the model include the Epiclastic and Rhyolite units. The critical slip surface on the provided pit design occurs throughout the overall slope with a FOS of 1.52. Changing the ISA within the Rhyolite to 51 degrees and within the Volcaniclastic and Epiclastic slopes to 50 degrees, results in a FOS of 1.34.

### **6.2.15 Section 15**

Section 15 is located on the southwestern side of JSLA pit. The cross section has a total wall height of approximately 834 feet, a slope dip direction of approximately 135 degrees, and an overall slope angle of 40 degrees. Major rock units present in the model include the Volcaniclastic, Epiclastic, and Andesite units. The critical slip surface on the provided pit design occurs throughout the overall slope with a FOS of 1.62. Changing the ISA within the Volcaniclastic and Epiclastic slopes to 51 degrees results in a FOS of 1.33.

## **7.0 BLASTING OPERATIONS**

### **7.1 Production Blasting**

The mining increment at Castle Mountain is expected to be 20 feet. A triple bench will be constructed leaving an adequate bench width to contain rock fall at 60-foot vertical intervals. For a 20-foot mining increment, a blasthole diameter of no more than 4 inches should be used to achieve optimum distribution of the explosive in the hole. Using a bench height to burden ratio (burden stiffness) of at least 2, and preferably 2.5 to 3.0, can be achieved with the 4-inch diameter hole. The burden should be no more than 10 feet, and 8 feet would be preferable. For the 10-foot burden, a spacing of 11.5 feet is reasonable. For the 8-foot burden, a spacing of 9.5 feet is reasonable. Sub-drilling 3 feet with 7 feet of stemming will provide good powder distribution to break the burden.

Explosive products are quite versatile and many suppliers can vary the specific gravity of the explosive product on the fly depending on the rock quality as measured by blast hole drilling parameters. Specific gravities ranging from 0.85 to 1.3 g/cc are available. Using a burden stiffness of 2, the range of powder factors that can be achieved with a 4-inch blasthole and the burden and spacing described above ranges from 0.87 lbs/yd<sup>3</sup> to 1.33 lbs/yd<sup>3</sup> (0.52- to 0.79- kg/m<sup>3</sup>), which should handle the majority of rock conditions experienced at Castle Mountain. The explosive loads per hole would range from 75 to 115 pounds per hole. Using a burden stiffness of 2.5, a powder factor of 1.3 lbs/yd<sup>3</sup> is obtained using the lowest density explosive product and the stemming depth detailed above.

### **7.2 Controlled Blasting**

Maintaining adequate catch bench widths for the recommended 48- to 52-degree interramp slope angles at the Castle Mountain Project will require carefully controlled blasting. It is recommended that the interramp slopes should be accomplished using pre-split blasting for a 60-foot-high triple bench. The pre-split should be drilled in a single pass to the full triple bench height and shot prior to the production shots on the first 20-foot mining increment of the triple bench.

Achieving the recommended interramp slope angles requires a bench face angle of 72 degrees that is reliable over 90 percent of the time for a 52-degree interramp slope angle. This

will result in a bench width of 27 feet, which is suitable for containing rock fall from the bench face above according to the modified Ritchie criterion. Past mining of the pits at Castle Mountain achieved these bench face angles with carefully controlled blasting even though the RQD of the rock mass is not exceptional. The jointing of the competent rhyolites and the chaotic nature of the clasts in the volcanoclastics and epiclastics was favorable to achieve steep bench face angles with pre-splitting. In some areas, the pre-split will not appear to have worked well, but in fact, it reduces the rock-mass damage and the benches will be more reliable.

Pre-split blasting initiates a crack defining the bench face and this linear blast pattern is initiated prior to the initiation of the production and buffer blast patterns. If a good crack forms, the vibrations of the main production blast are reflected back into the rock mass, protecting the rock forming the bench face.

Pre-split blasting adds cost to the blasting operation, but the benefit achieved by allowing steeper interramp angles with higher bench reliability is far greater than the additional cost. The cost of pre-splitting is a linear function based on the length of the pre-split blast patterns. The savings in stripping costs resulting from the steeper interramp slope angles that are achievable with the careful pre-split blasting increase as a geometric function (cubic volumetric function). Figure 7-1 displays this concept. This figure was generated in 2004, so the costs are outdated; however, the savings resulting from pre-splitting by increasing the interramp slope angle from 40 degrees to 45 degrees over a 1000-foot-long sector of a pit is significantly greater than the cost of pre-splitting.

### ***7.2.1 Initial Pre-Split Blasting Recommendation***

Drills using down-hole hammers have worked well for the pre-split operations. The Atlas Copco ROC L6 is quite flexible and is capable of drilling 3.5- to 5.125-inch-diameter holes. These rigs can drill angled holes, and many times steeply inclined pre-split holes function better than vertical holes. Rigs that can drill accurately for a full 60-foot-high triple bench height should be obtained. In some cases, the drill rigs used for production blasting can drill vertical holes over the full triple bench height at hole diameters less than 5 inches. These rigs may work quite well for the pre-splitting operation and allow the operator to use the same equipment for pre-splitting and production. However, when estimating the capital costs for drill machines, the pre-split operation must be considered to obtain adequate availability of rigs for this operation.

Experimentation of several pre-split blast patterns will have to be performed to arrive at the optimum pattern at Castle Mountain. The pattern may change as a function of wall orientation and the orientation of the geologic fabric. An initial recommendation for a pre-split pattern would consist of 4-inch-diameter holes drilled with a spacing of 5 feet. The triple bench pre-split should be drilled at -80 degrees from horizontal with 2 feet of sub-drill for a total of 63 feet, accounting for the hole inclination. A 1.125-inch-diameter packaged pre-split explosive such as Orica's Powersplit is recommended to provide good charge distribution. It is recommended to not load the bottom of a large diameter hole with an equivalent charge and detonate with a booster, as this does not provide a good pre-split. This pre-split product is an emulsified explosive in continuous tube packaging.

The Orica product has a 10 g/m detonating cord running through the center of the product to ensure fast detonation of the product. The upper 3.5 feet of the hole should not be charged. To avoid a hard toe, double over the packaged explosive to double the charge in the lower 5 feet of the hole. If stemming is used, a hole plug should be set at roughly 3.5 feet of depth and good stemming material should be placed on top of the plug. Using the 1.125-inch-diameter continuous pre-split product would provide a load of roughly 35 pounds per hole. This design should provide a shear factor of 0.10 lbs/ft<sup>2</sup>. This charge should work well but may have to be adjusted depending on the rock quality. As mentioned above, the pre-split should be shot well before the production and buffer row shots. A minimum of 5 pre-split holes should be fired on the same delay.

### ***7.2.2 Initial Buffer Blasting Recommendation***

Buffer blasting should be performed to minimize damage to the bench faces. Ideally, a blast damage zone around the typical production blast should be defined by near-field vibration monitoring and by drilling some holes in proximity to (but not within) the blast pattern, to measure crack dilation with a pre- and post-blast televiewer survey (a dummy tool should be run before the televiewer to make sure the holes are safe to run the televiewer tool). McKenzie and Holley (2004) authored a paper detailing damage related to blasting. They drilled holes near vibration monitoring stations and used video cameras to record the pre- and post-blast crack development to be correlated with measured particle velocities. Their conclusions included the following:

1. “Observable damage, in the form of new or open cracks, appears to commence at around 200 mm/s (7.9 ips).”
2. “Once levels increase to around 400 mm/s (15.7 ips), observable damage can become intense.”
3. “Damage in the inspection holes was observed over the full depth of the holes.”
4. “With large diameter blast holes, normal charge weights and normal stand-off distances from the designed pit wall, this level of control cannot be achieved.”

Ideally, vibration levels behind the pre-split line at the designed mid-bench should be lower than 15 inches per second.

Although pre-splits will help cushion the blast vibrations from the production shot, the damage zone should be estimated to help develop a buffer blast pattern to make sure damage to the bench face, and particularly the bench crest, are minimized. The buffer blast should be shot as a four-row rind shot to a free face. The shovel or loader should make a pass to develop this rind shot, which should consist of three buffer rows and one production row. With a 20-foot mining increment, the production hole diameter should be no greater than 4 inches to achieve good explosive distribution and optimum breakage of the rock. The burden and spacing is reduced to give good breakage of the beam of rock in the blast burden. With the recommended burdens and spacings for the rind shot given below, there is good charge distribution for breaking the rock and imparting minimal damage to the bench face. A burden stiffness of 2.5 for the three buffer rows as a starting point recommendation is described below.

1. The buffer shot pattern in order from pre-split line:
  - a. First buffer row: 8.0 feet from pre-split, 9.5-foot spacing, 51 pounds of charge (0.85g/cc SG of explosive), hole plug set at 7 feet with good quality stemming in a 4-inch-diameter drill hole, **no sub drilling on third increment**. Otherwise, use 3 feet of sub-drill.
  - b. Second buffer row: 16 feet from pre-split, 9.5-foot spacing, 51 pounds of charge, hole plug set at 7 feet with good quality stemming in a 4-inch-diameter drill hole, **no sub drilling on third increment**. Otherwise, use 3 feet of sub-drill.
  - c. Third buffer row: 24 feet from pre-split, 9.5-foot spacing, 51 pounds of charge, hole plug set at 7 feet with good quality stemming in a 4-inch-diameter drill hole, **no sub drilling on third increment**. Otherwise, use 3 feet of sub-drill.
  - d. Standard production charge set at 32 feet from pre-split, 10-foot burden, 11.5-foot spacing, 87 to 96 pounds of charge (1.0 to 1.1 SG of explosive), 7 feet of good quality stemming in a 4-inch-diameter hole, **no sub drilling on third increment**. Otherwise, use 3 feet of sub-drill. On the third increment with no sub-drill, to get the required load, a 1.3 g/cc SG explosive will be used.

The layout for this initial controlled blast design is shown in Figure 7-2. The timing of the buffer shots should be designed such that there is a minimum of 12 milliseconds of delay between each blast hole being detonated, and 20 to 40 milliseconds between rows.

### **7.2.3 *Controlled Blast Audits***

The excavated benches should be audited on a routine basis to make sure that the bench widths and bench face angles are performing to expectations. Each blast design that impacts a final wall should be documented and data, including the rock type, alteration type, persistent joint systems, controlled blast design with spacing and burden dimensions for buffer and pre-split rows, vibration levels, and cumulative bench face angle plots derived from drone scans, should be collected. Overlapping drone imagery should be collected at a minimum of quarterly to generate three-dimensional point clouds that are used to audit the bench face angles and bench widths. Adjustments to the blast design will have to be made, if the bench face angles and catch bench widths are lower than predicted. Additionally, the drone scans will help determine if the design toes are accomplished. If hard toes are noticed, adding more powder the bottom of the pre-split row or increasing the sub-drill of the pre-split holes may be required. Figure 7-3 shows an example of a bench face angle audit compared to the expected bench face angle distribution determined by the Backbreak analysis.

## **REFERENCES**

McKenzie, C.K. & Holley, K. 2004, 'A study of damage profiles behind blasts' in Proceedings of the 30th Annual Conference on Explosives and Blasting Techniques, International Society of Explosives Engineers, vol. 2.

# CALL & NICHOLAS, INC.

2475 N. Coyote Dr.  
Tucson, Arizona 85745 U.S.A.

---

Tel: 520.670.9774  
Fax: 520.670.9251  
E-Mail: cni@cnitucson.com

*Principals*  
T. M. Ryan  
R. W. Pratt  
L. R. Standridge  
N. A. Asbury  
S. D. Cylwik

## MEMORANDUM

**To:** Doug Moore, Project Manager / Equinox Gold Corp  
Aren Hall, Environmental & Permitting Manager / Equinox Gold Corp

**From:** Daniel Childs, Geological Engineer / Call & Nicholas, Inc.  
Scott Cylwik, P.E., Vice President / Call & Nicholas, Inc.

**Date:** 22 June 2023

**Subject:** Castle Mountain – South Extension Pit Slope Stability Update

---

### 1.0 EXECUTIVE SUMMARY

At the request of Aren Hall and Doug Moore of Equinox Gold Corp (EQX), the South Extension pit, as a portion of the 2020 Call & Nicholas, Inc. (CNI) report titled *Castle Mountain Geotechnical Feasibility Report*, was re-analyzed using updated groundwater conditions.

EQX was provided with a memo by Clear Creek Associates titled *Evaluation of Dewatering Requirements and an Updated Simulation of a Pit Lake* on May 18, 2023, that estimates pit dewatering conditions at various stages of the mining process. CNI used the estimated 2050 groundwater surface to update the overall slope stability models of the South Extension pit to investigate the potential impact that may be encountered.

Based on the provided data, the 2050 groundwater surface assumption does not impact the Factor of Safety (FoS) of the South Extension ultimate pit design model when considering global stability with two-dimensional limit-equilibrium. If groundwater conditions are different than what has been provided, then stability for the overall pit may be affected.

### 2.0 GROUNDWATER MODEL

Clear Creek Associates provided CNI with estimated three-dimensional groundwater surfaces for the end of each major mining stage, as follows:

- 2030 – JSLA
- 2033 – Jumbo/Oro Belle

- 2036 – Jumbo/Oro Belle (east)
- 2042 – South Extension
- 2050 – South Extension at Maximum

The original scope of work for the 2020 CNI study focuses on the stability of the final pit design, and the interaction of groundwater and slope stability at interim stages was not analyzed.

### 3.0 OVERALL SLOPE STABILITY ANALYSIS

Sections 1, 2, 3, 5, and 6 in the 2020 CNI study are located at key positions around the South Extension pit, as presented in Figure 6-1 from that report.

#### 3.1 Results

The results from the updated analyses are presented in **Table 3-1**. The only change in FoS values from the 2020 study is the Section 5 as-designed model. A slight reduction in FoS from 1.35 to 1.31 was found when re-analyzing the model. The slip surface does not intercept the 2050 groundwater surface, so the change is attributed to changes in the Rocscience Slide2 optimization methods. FoS estimates still meet all design acceptance criteria.

**Table 3-1. Overall Stability Analyses Results**

| Section | FOS                |                             |
|---------|--------------------|-----------------------------|
|         | 2020 Study Results | Updated Groundwater Results |
| 1       | 1.34               | 1.34                        |
| 2       | 1.56               | 1.56                        |
| 3       | 1.32               | 1.32                        |
| 5       | 1.35               | 1.31                        |
| 6       | 1.59               | 1.59                        |

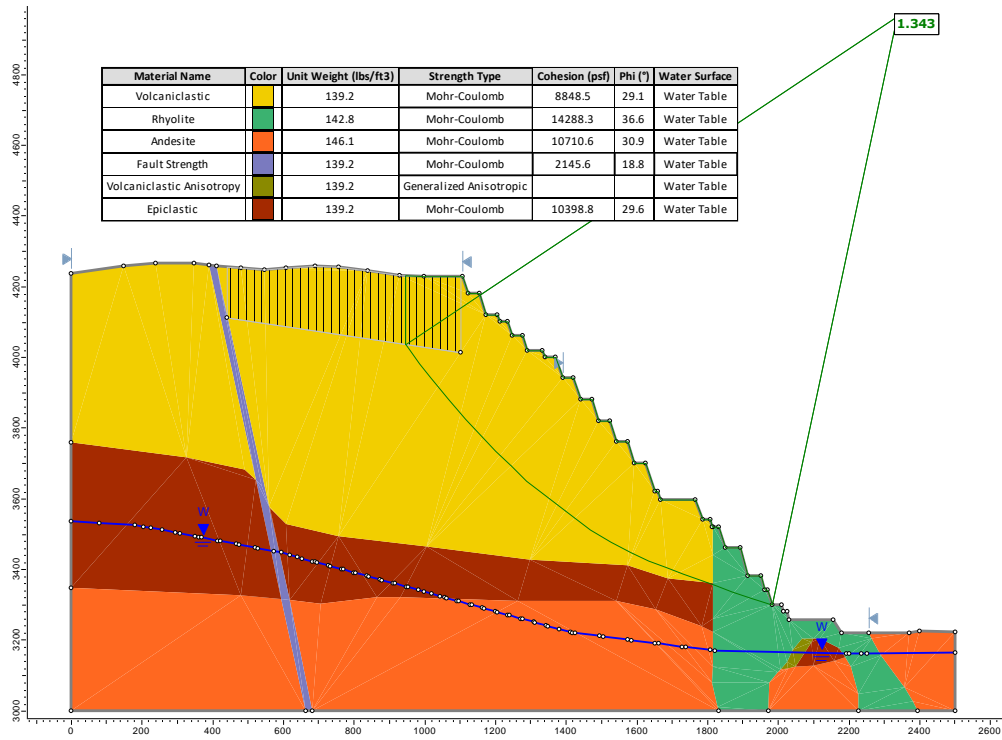


Figure 3-1. Section 1 – As Designed

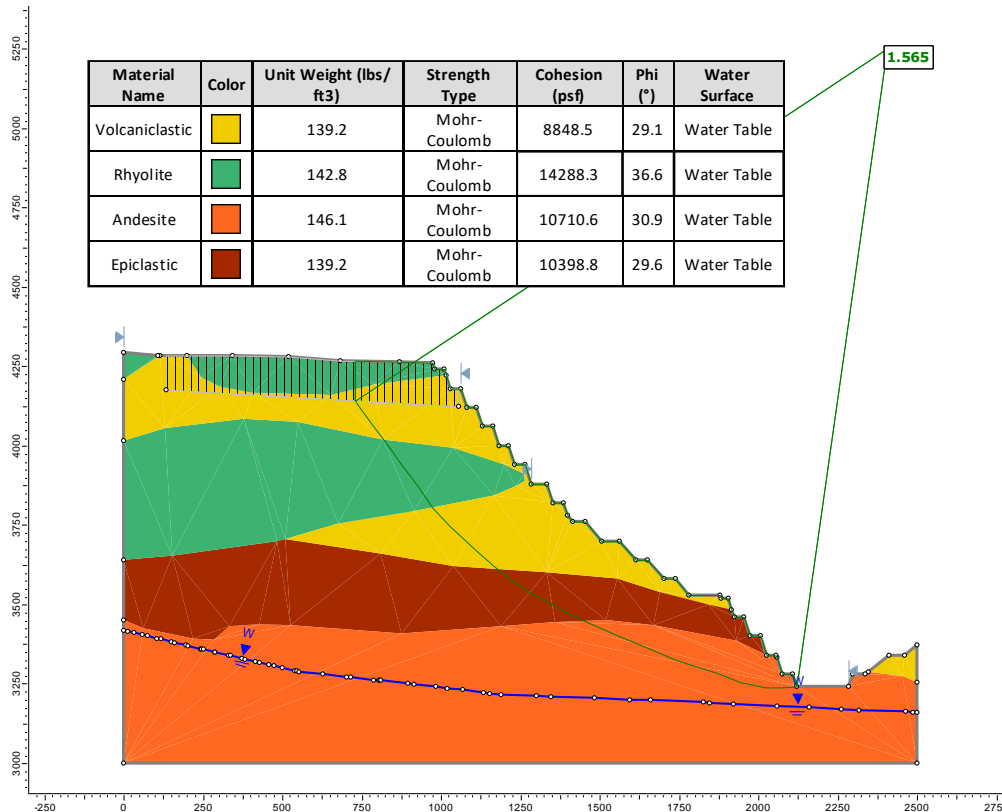


Figure 3-2. Section 2 – As Designed

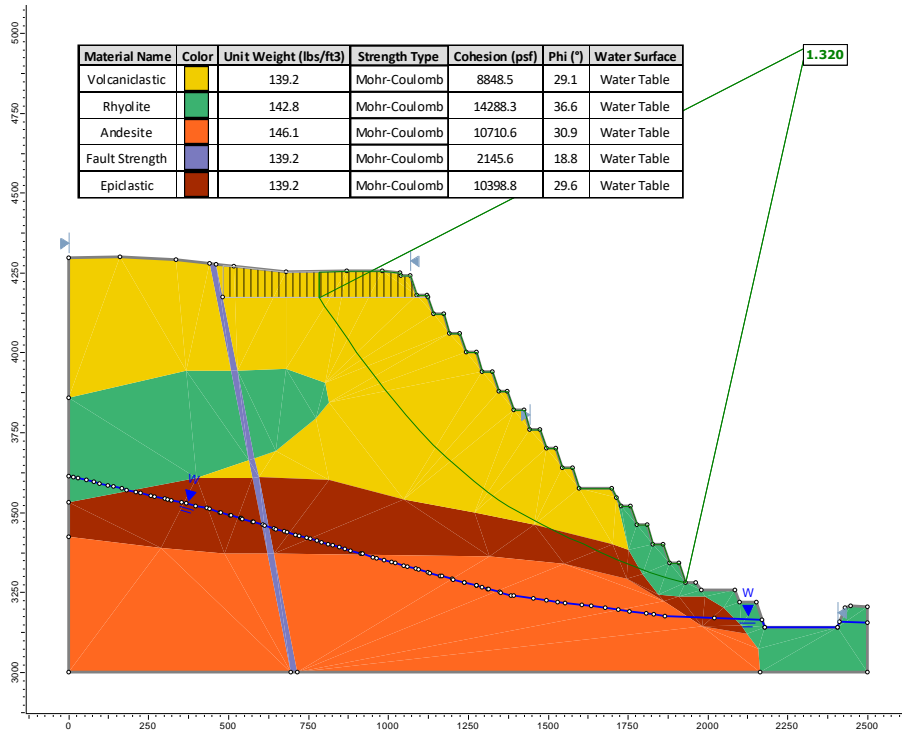


Figure 3-3. Section 3 – As-Designed

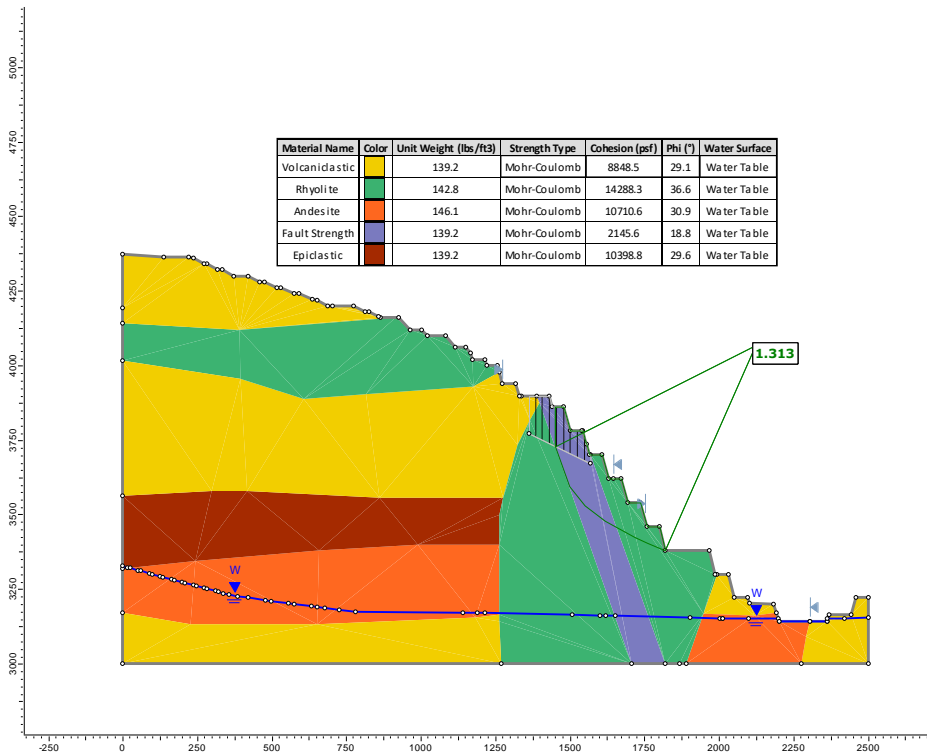


Figure 3-4. Section 5 – As-Designed

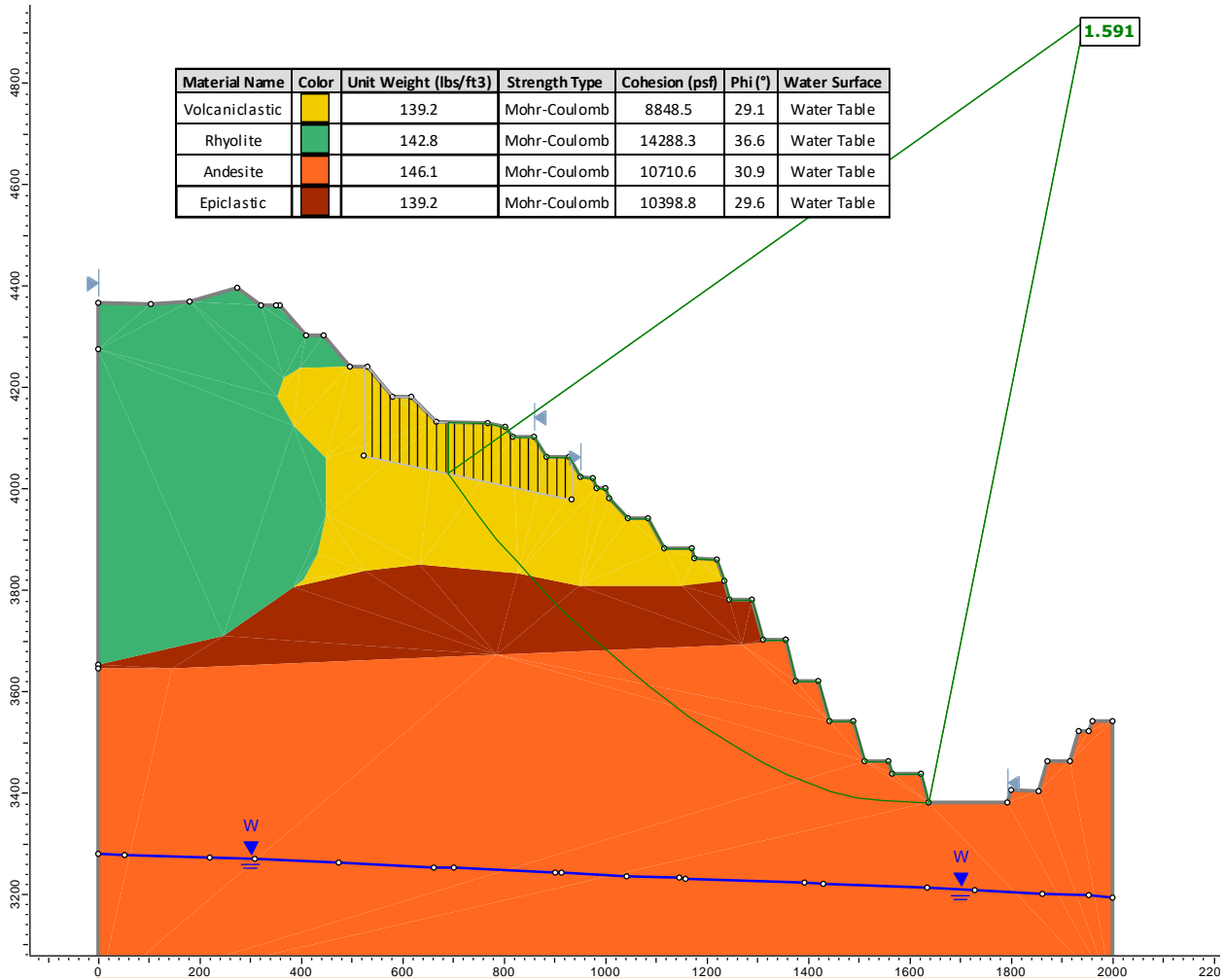


Figure 3-5. Section 6 – As-Designed

# CALL & NICHOLAS, INC.

2475 N. Coyote Dr.  
Tucson, Arizona 85745 U.S.A.

---

Tel: 520.670.9774  
Fax: 520.670.9251  
E-Mail: cni@cnitucson.com

Principals  
T. M. Ryan  
R. W. Pratt  
L. R. Standridge  
N. A. Asbury  
S. D. Cylwik

## MEMORANDUM

**To:** Doug Moore, Project Manager / Equinox Gold Corp  
Aren Hall, Environmental & Permitting Manager / Equinox Gold Corp

**From:** Daniel Childs, Geological Engineer / Call & Nicholas, Inc.  
Scott Cylwik, P.E., Vice President / Call & Nicholas, Inc.

**Date:** 01 July 2024

**Subject:** Castle Mountain – March 2022 Pit Design Geotechnical Verification

---

### 1.0 EXECUTIVE SUMMARY

At the request of Equinox Gold Corp (EQX), Call & Nicholas, Inc. (CNI) has performed a geotechnical design verification of the March 2022 pit design. The design verification includes reviewing designed interramp slope angles to verify that design recommendations were followed from the 2020 CNI report titled *Castle Mountain Geotechnical Feasibility Report* and running two-dimensional limit-equilibrium (2DLE) models on critical cross sections to verify that Factor of Safety (FoS) estimates meet or exceed minimum design acceptance criteria. Additionally, groundwater surfaces provided by Clear Creek Associates were used to simulate groundwater conditions at the completion of various stages of mining and in a new scenario where the pits are not backfilled and pit lakes are allowed to form.

Based on the data available to CNI at the time of analysis, all analyzed slopes (except “Section 6 – East” which is in the “ISA\_ISLAND” domain) meet or exceed a 1.20 FoS. Reducing the slope in Section 6 - East from the 4470-foot elevation to a 4410-foot elevation increases the FoS from 1.11 to 1.20 and meets the minimum FoS requirements. Additionally, plans provided by EQX to CNI indicate that the critical infrastructure near the south extension pit is located outside the recommended 300-foot exclusionary boundary and the updated 2DLE model does not indicate that the critical infrastructure will be impacted by potential overall slope instabilities.

## 2.0 GROUNDWATER MODEL

Clear Creek Associates provided CNI with estimated three-dimensional groundwater surfaces for the end of each major mining stage, as follows:

- 2030 – JSLA
- 2033 – Jumbo/Oro Belle
- 2036 – Jumbo/Oro Belle (east)
- 2042 – South Extension
- 2050 – South Extension at Maximum

The relevant groundwater surfaces used in each analyzed cross sections is presented in Table 2-1.

**Table 2-2. Overall Stability Analyses Results**

| <b>Section</b> | <b>Zone</b>                 | <b>Mining Stage</b> | <b>Estimated Year of Mining Stage Completion</b> |
|----------------|-----------------------------|---------------------|--|
| 1              | South Extension Pit         | 6F                  | 2042   |
| 2              | South Extension Pit - North | 6B                  | 2030   |
| 3              | JSLA Pit                    | 6B                  | 2030   |
| 4              | JSLA Pit                    | 6B                  | 2030   |
| 5              | Oro Belle Pit               | 6D                  | 2036   |
| 6 - East       | Oro Belle Pit               | 6D                  | 2036   |
| 6 - West       | Jumbo Pit                   | 6C                  | 2033   |
| 7              | Jumbo Pit                   | 6C                  | 2033   |
| 8              | Oro Belle Pit               | 6D                  | 2036   |
| 9              | Oro Belle Pit               | 6D                  | 2036   |

## 3.0 OVERALL SLOPE STABILITY ANALYSIS

Sections 1 through 9 were selected based on results from the 2020 CNI study and were modified based on the updated pit geometry. The cross sections located on a plan map are presented in Figure 3-1.

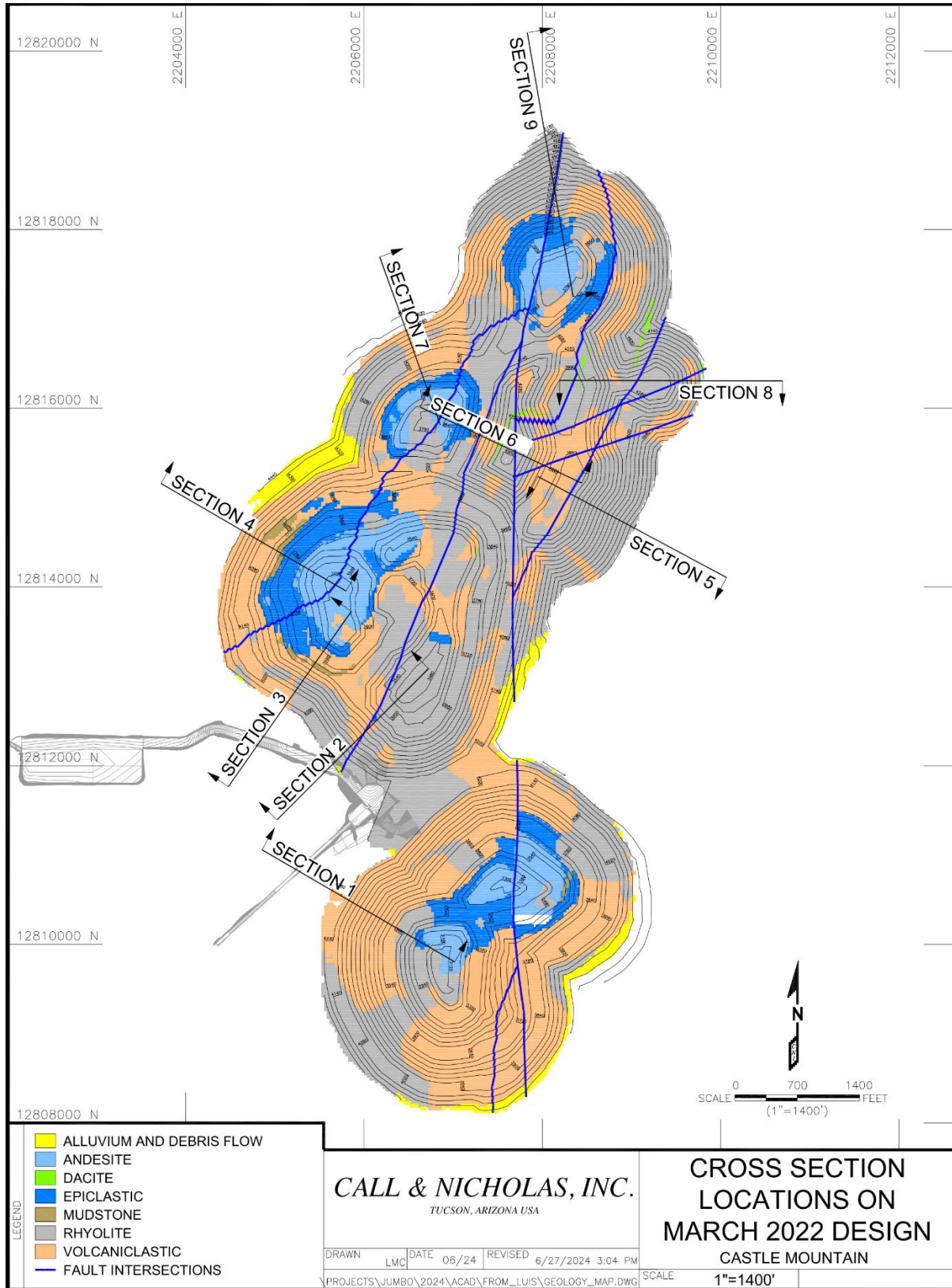


Figure 3-1. Cross Section Locations on March 2022 Design

### 3.1 **Results**

The results from the 2DLE analyses are presented in Table 3-1. Using the provided design, Section 6 – East results in a FoS of 1.11 for both water scenarios; however, by reducing the slope elevation from 4470 feet to 4410 feet, the FoS increases to 1.20. Assuming this design change takes place, all FoS estimates will meet design acceptance criteria of having an FoS of greater than or equal to 1.20 for both the estimated water conditions and pit lake conditions. The estimated FoS values are highly dependent on the interpreted location of fault planes. The locations of modeled faults should be updated regularly once mining begins, and slope stability analyses will need to be updated accordingly if modeled fault locations change or new faults are identified.

**Table 3-1. Overall Stability Analyses Results**

| Section  | Zone                        | Factor of Safety   |                                |
|----------|-----------------------------|--------------------|--------------------------------|
|          |                             | At Estimated Water | Pit Lake Scenario (2023 Water) |
| 1        | South Extension Pit         | 1.26               | 1.31                           |
| 2        | South Extension Pit - North | 1.55               | 1.50                           |
| 3        | JSLA Pit                    | 1.24               | 1.43                           |
| 4        | JSLA Pit                    | 1.29               | 1.59                           |
| 5        | Oro Belle Pit               | 1.60               | 1.60                           |
| 6 - East | Oro Belle Pit               | 1.20*              | 1.20*                          |
| 6 - West | Jumbo Pit                   | 1.61               | 1.60                           |
| 7        | Jumbo Pit                   | 1.48               | 1.48                           |
| 8        | Oro Belle Pit               | 1.94               | 1.94                           |
| 9        | Oro Belle Pit               | 1.45               | 1.45                           |

\* The FoS for this section assumes that the elevation of this slope is reduced from the 4470-foot elevation to 4410-foot elevation

### 3.1.1 Section 1

Section 1 is located on the northwestern portion of the South Extension Pit. The critical infrastructure of interest is located roughly 570 feet from the crest of the slope and no slip surfaces extended beneath it. For the 2042 and 2023 (Pit Lake) water condition scenarios, the FoS is 1.26 and 1.31, and the resulting slip surfaces are presented in **Figure 3-2** and **Figure 3-3**, respectively.

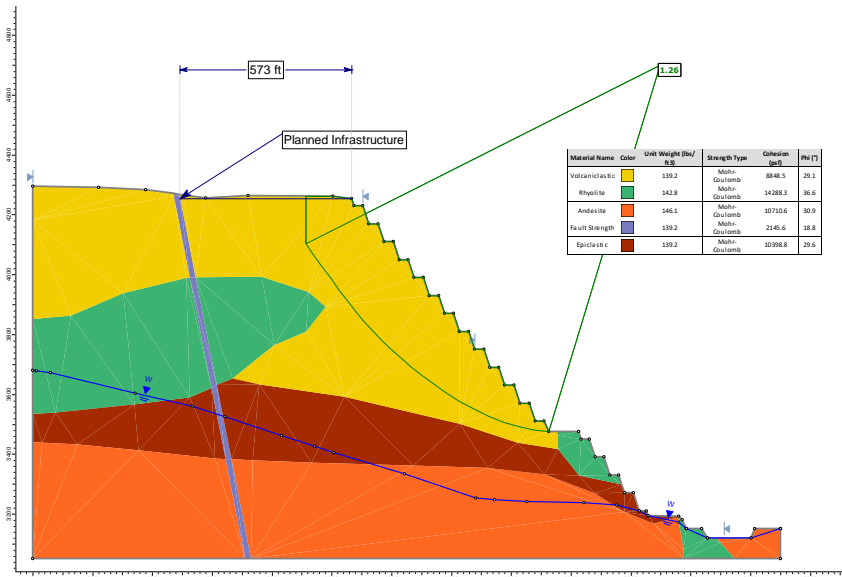


**Figure 3-2. Section 1, Assuming 2042 Water Surface**

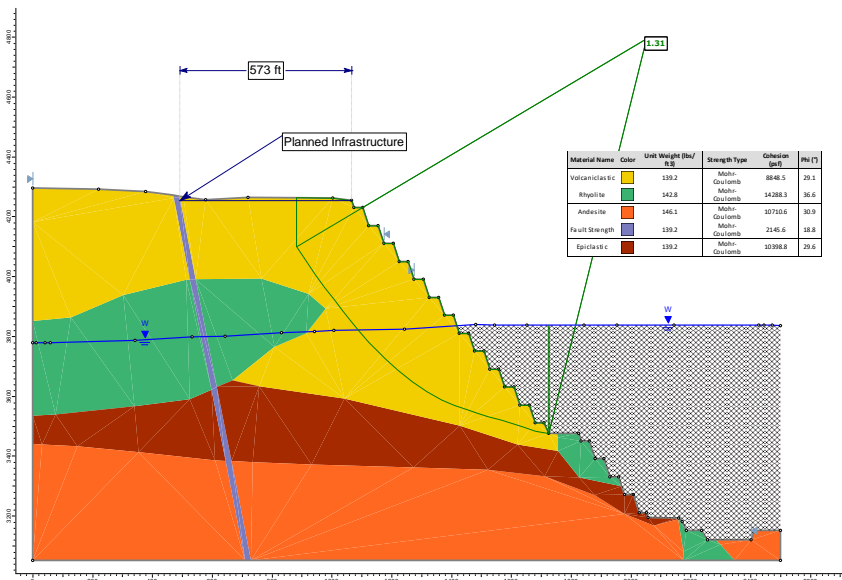


**Figure 3-3. Section 1, Assuming 2023 Water Surface**

**3.1.2 Section 2**

Section 2 is located on the southwest wall of the northern end of the South Extension Pit. For the 2030 and 2023 (Pit Lake) water condition scenarios, the FoS is 1.50 and 1.55, and resulting slip surfaces are presented in Figure 3-4 and Figure 3-5, respectively

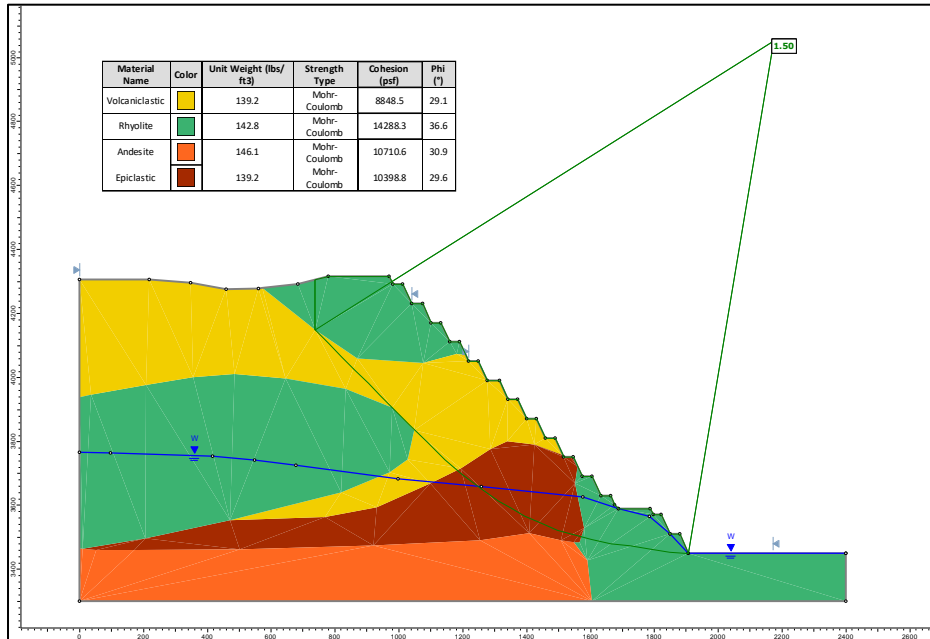


**Figure 3-4. Section 2, Assuming 2030 Water Surface**

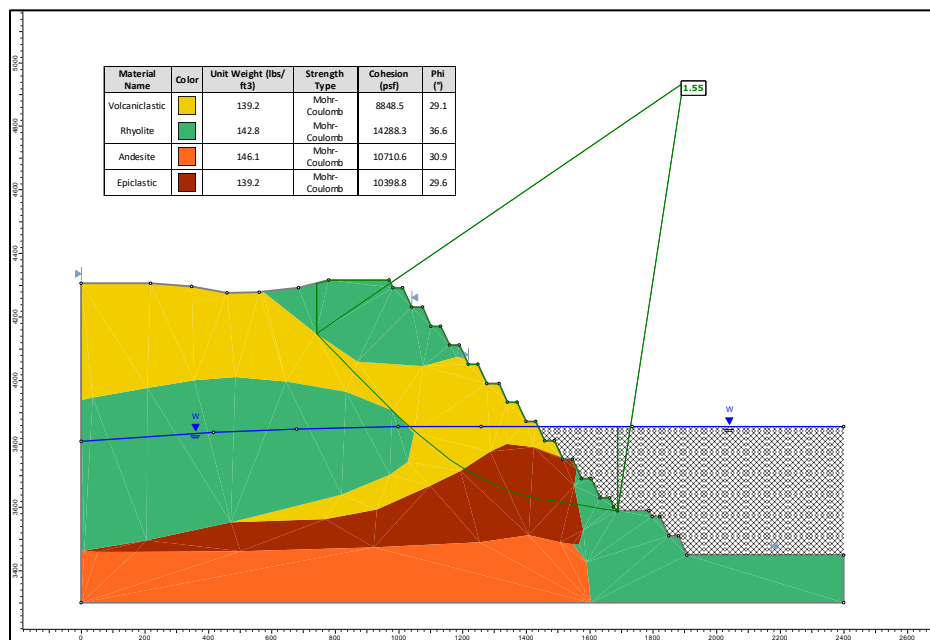


**Figure 3-5. Section 2, Assuming 2023 Water Surface**

### 3.1.3 Section 3

Section 3 is located on the southwest wall of the JSLA Pit. For the 2030 and 2023 (Pit Lake) water condition scenarios, the FoS is 1.24 and 1.43, and resulting slip surfaces are presented in Figure 3-6 and Figure 3-7, respectively.

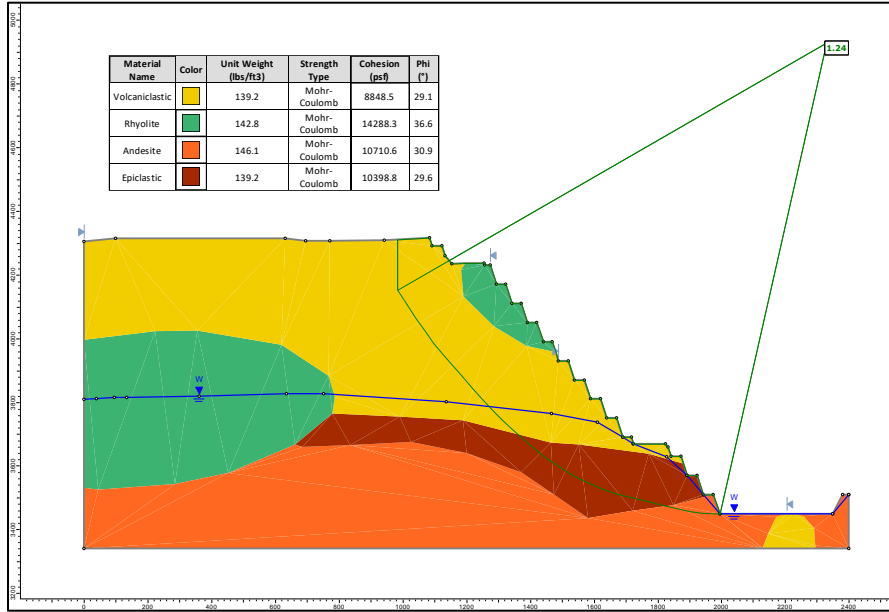


**Figure 3-6. Section 3, Assuming 2030 Water Surface**

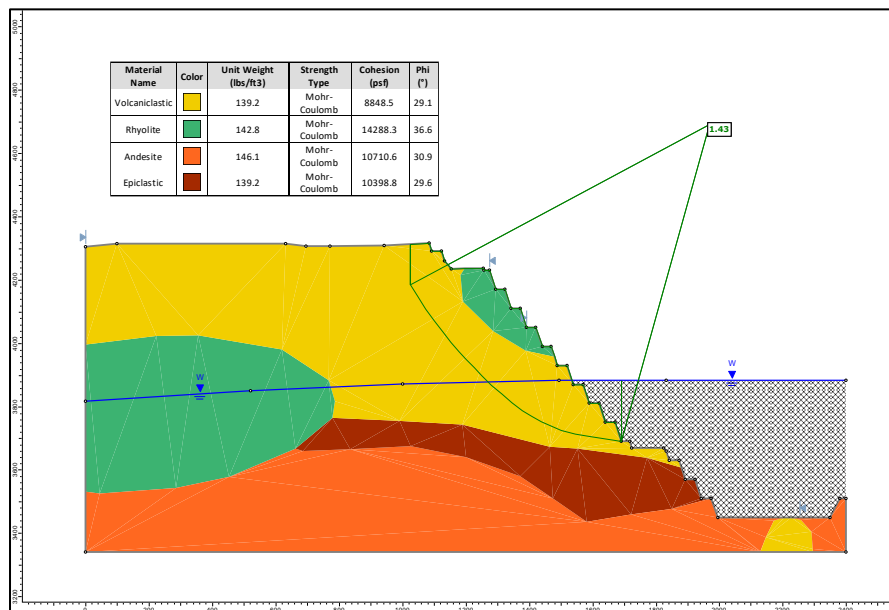


**Figure 3-7. Section 3, Assuming 2023 Water Surface**

### 3.1.4 Section 4

Section 4 is located on the northwest wall of the JSLA Pit. For the 2030 and 2023 (Pit Lake) water condition scenarios, the FoS is 1.29 and 1.59, and resulting slip surfaces are presented in **Figure 3-8** and **Figure 3-9**, respectively.

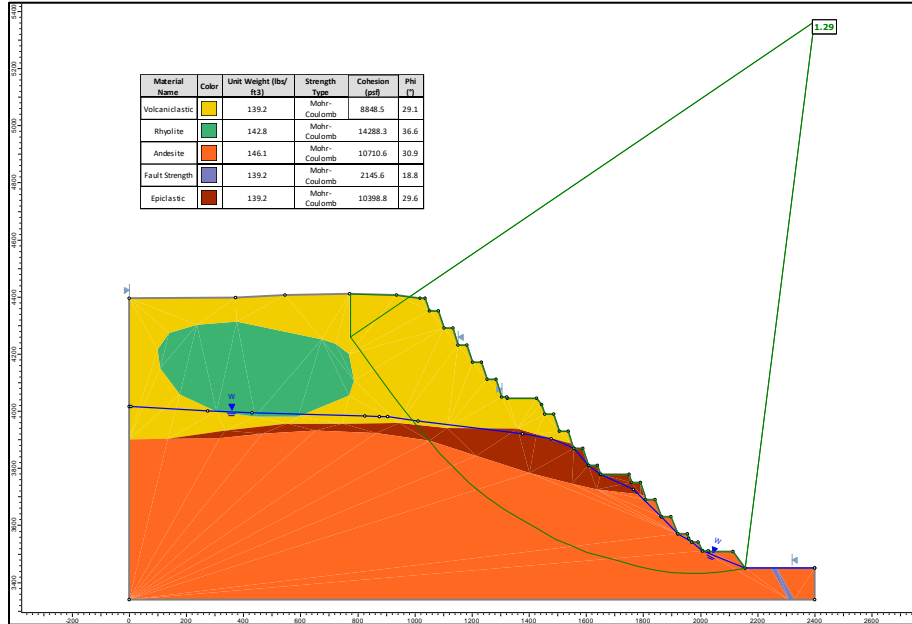


**Figure 3-8. Section 4, Assuming 2030 Water Surface**

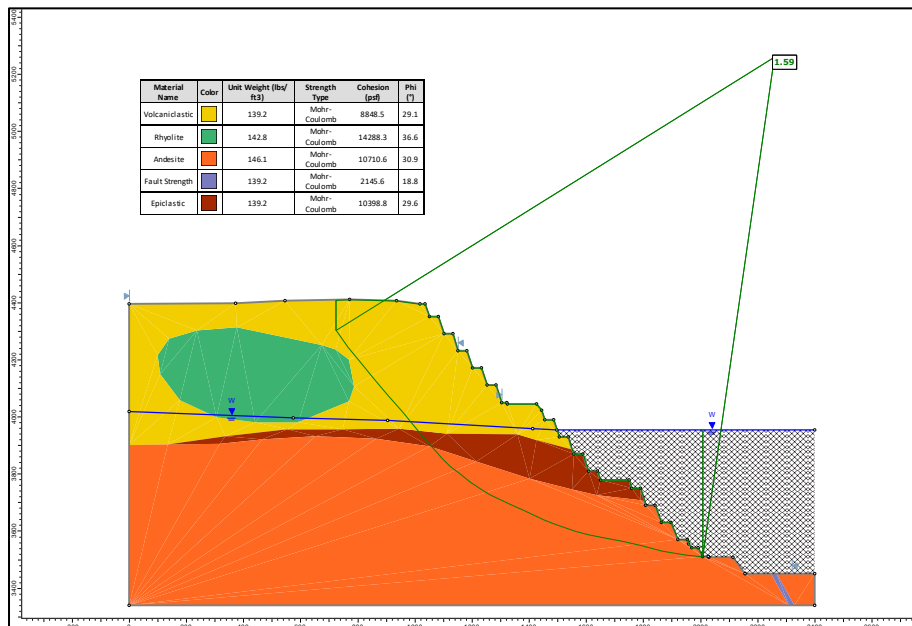


**Figure 3-9. Section 4, Assuming 2023 Water Surface**

### 3.1.5 Section 5

Section 5 is located on the southeast wall of the Oro Belle Pit. For the 2036 and 2023 (Pit Lake) water condition scenarios, the FoS is 1.60 and 1.60, and resulting slip surfaces are presented in **Figure 3-10** and **Figure 3-11**, respectively.

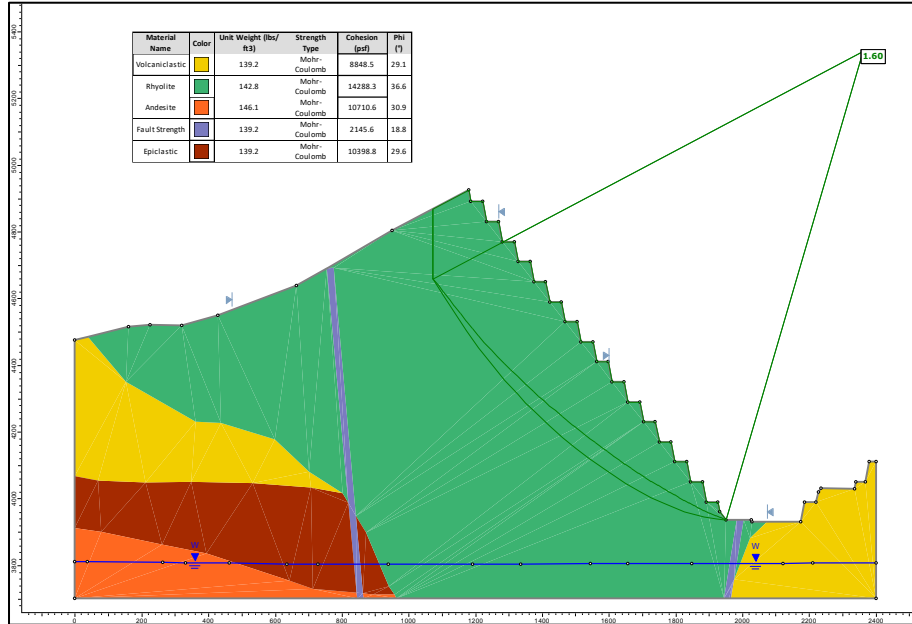


**Figure 3-10. Section 5, Assuming 2036 Water Surface**

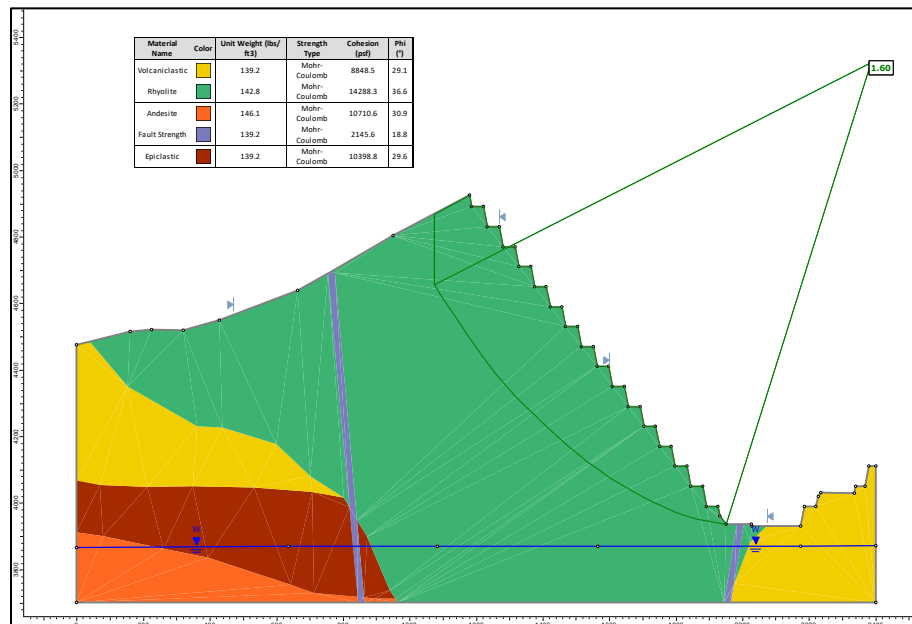


**Figure 3-11. Section 5, Assuming 2023 Water Surface**

### 3.1.6 Section 6 - East

Section 6 - East is located on the west wall of the Oro Belle Pit. For the 2036 and 2023 (Pit Lake) water condition scenarios, the FoS of the provided design is 1.11 and 1.11, and resulting slip surfaces are presented in **Figure 3-12** and **Figure 3-13**, respectively. By decreasing the slope height to 4410 feet instead of 4470 feet, the FoS is increased to 1.20, as shown in **Figure 3-14**.

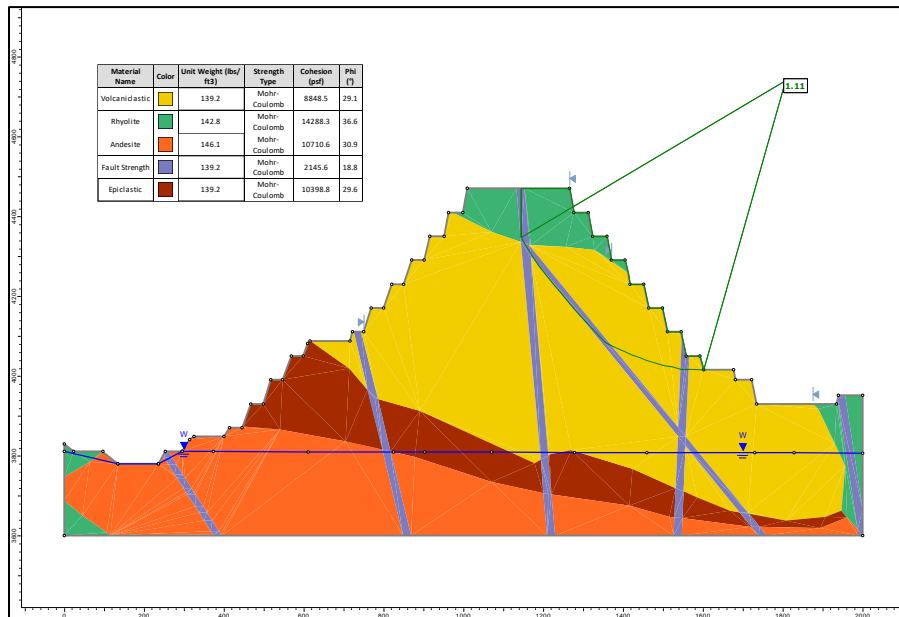


**Figure 3-12. Section 6 – East, Assuming 2036 Water Surface**

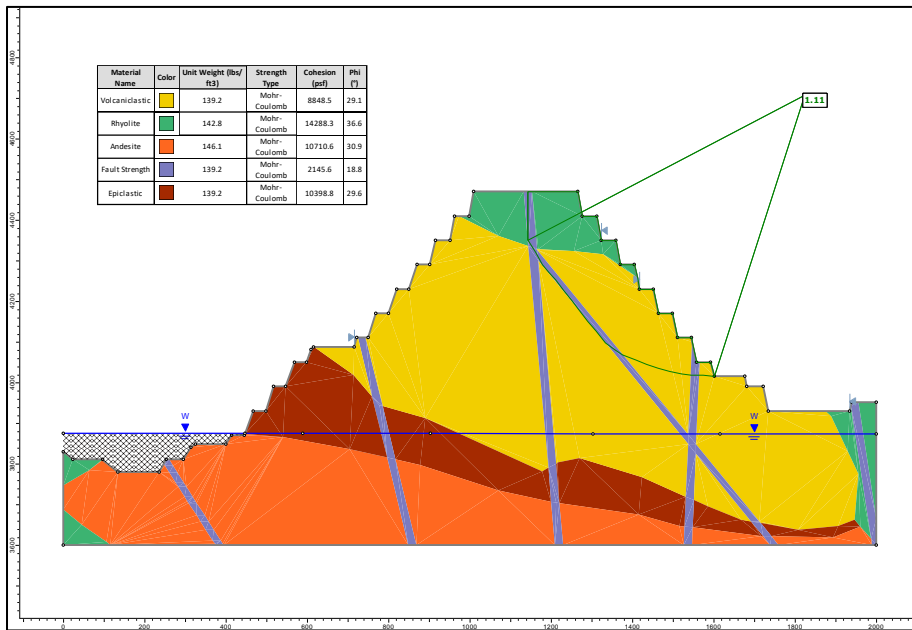


Figure 3-13. Section 6 – East, Assuming 2023 Water Surface

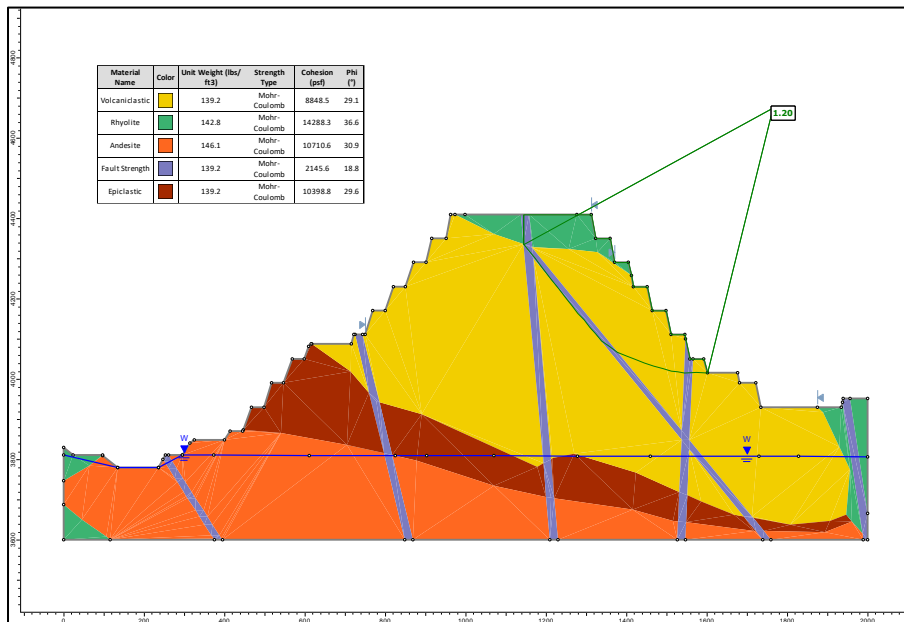
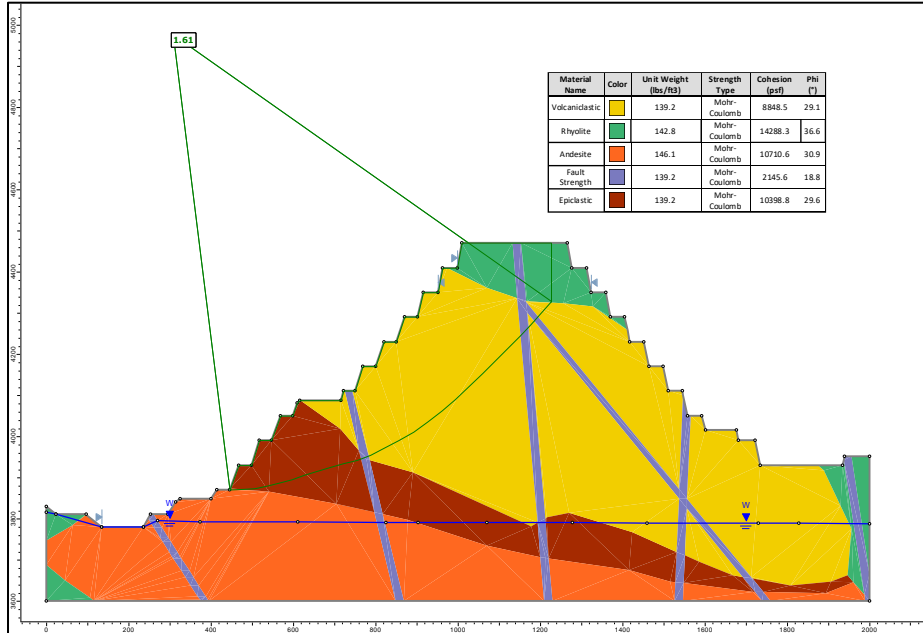


Figure 3-14. Section 6 – East, Assuming 2036 Water Surface (Modified Design)

**3.1.7 Section 6 - West**

Section 6 - West is located on the eastern wall of the Jumbo Pit. For the 2033 and 2023 (Pit Lake) water condition scenarios, the FoS is 1.61 and 1.60, and resulting slip surfaces are presented in **Figure 3-15** and **Figure 3-16**, respectively.



**Figure 3-15. Section 6 – West, Assuming 2033 Water Surface**

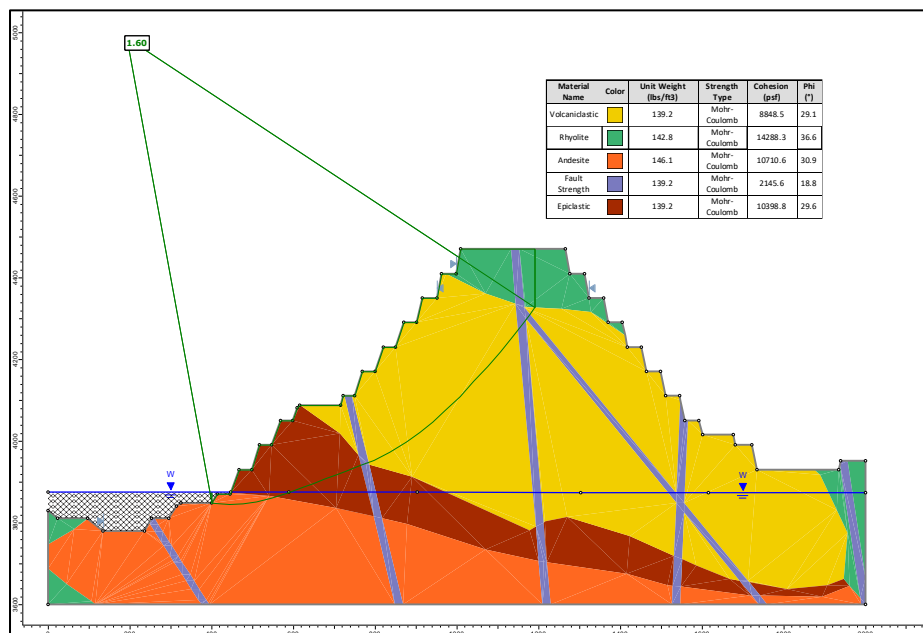


**Figure 3-16. Section 6 – West, Assuming 2023 Water Surface**

### 3.1.8 Section 7

Section 7 is located on the northwest wall of the Jumbo Pit. For the 2033 and 2023 (Pit Lake) water condition scenarios, the FoS is 1.48 and 1.48, and resulting slip surfaces are presented in **Figure 3-17** and **Figure 3-18**, respectively.

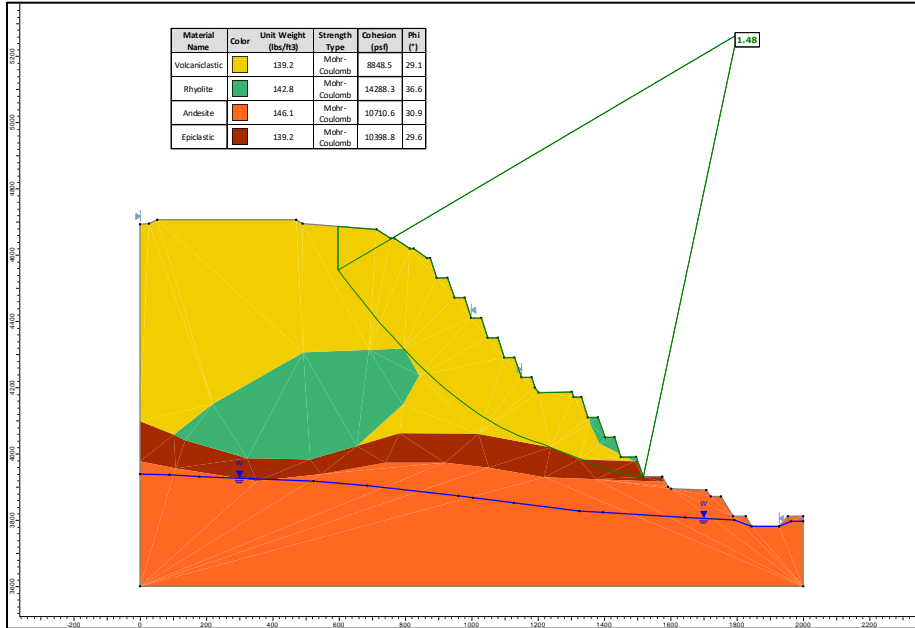


**Figure 3-17. Section 7, Assuming 2033 Water Surface**

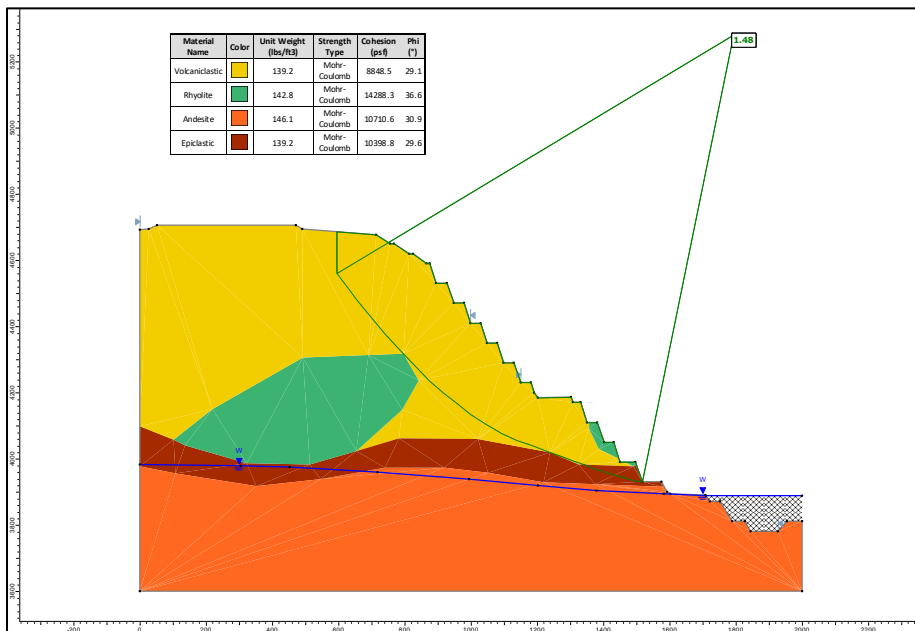


**Figure 3-18. Section 7, Assuming 2023 Water Surface**

**3.1.9 Section 8**

Section 8 is located on the east wall of the Oro Belle Pit. For the 2036 and 2023 (Pit Lake) water condition scenarios, the FoS is 1.94 and 1.94, and resulting slip surfaces are presented in **Figure 3-19** and **Figure 3-20**, respectively.

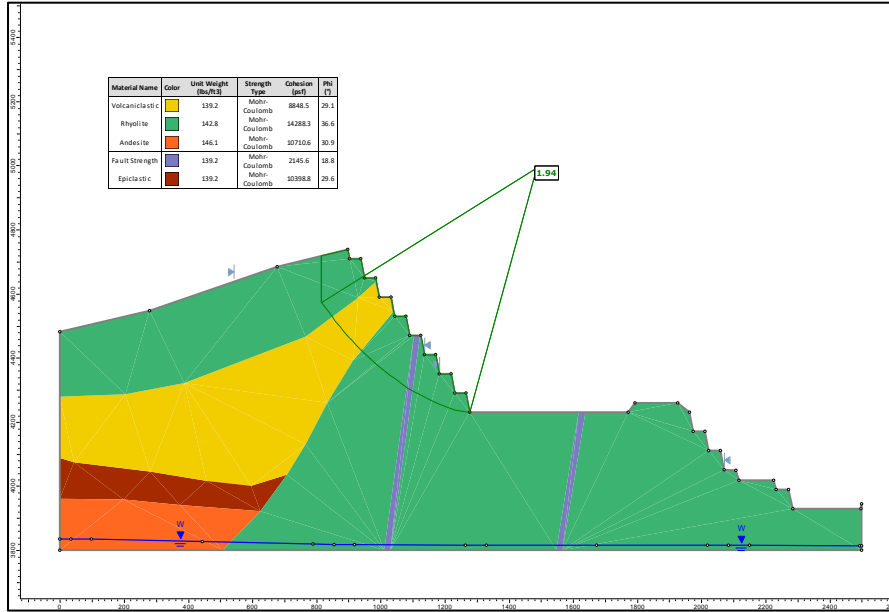


**Figure 3-19. Section 8, Assuming 2036 Water Surface**

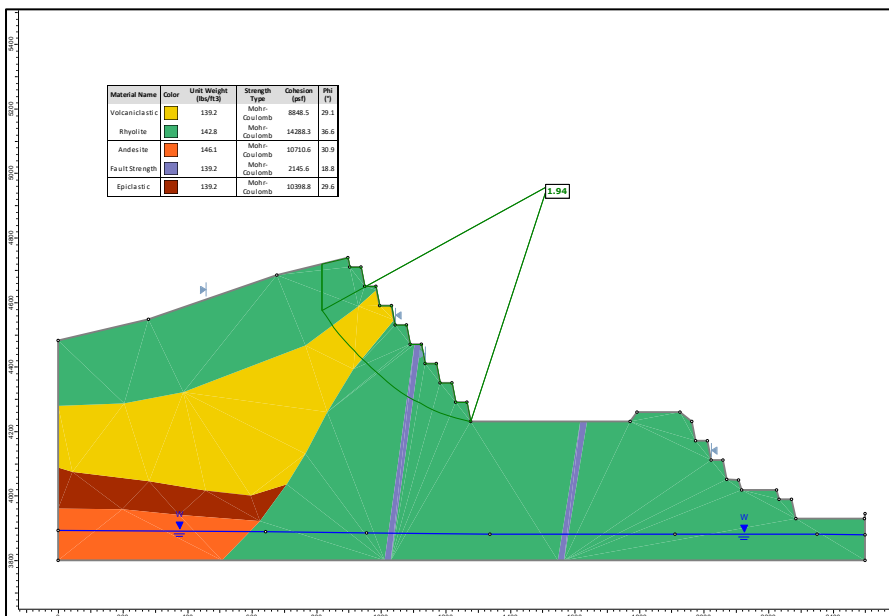


**Figure 3-20. Section 8, Assuming 2023 Water Surface**

**3.1.10 Section 9**

Section 9 is located on the north wall of the Oro Belle Pit. For the 2036 and 2023 (Pit Lake) water condition scenarios, the FoS is 1.45 and 1.45, and resulting slip surfaces are presented in **Figure 3-21** and **Figure 3-22**, respectively.

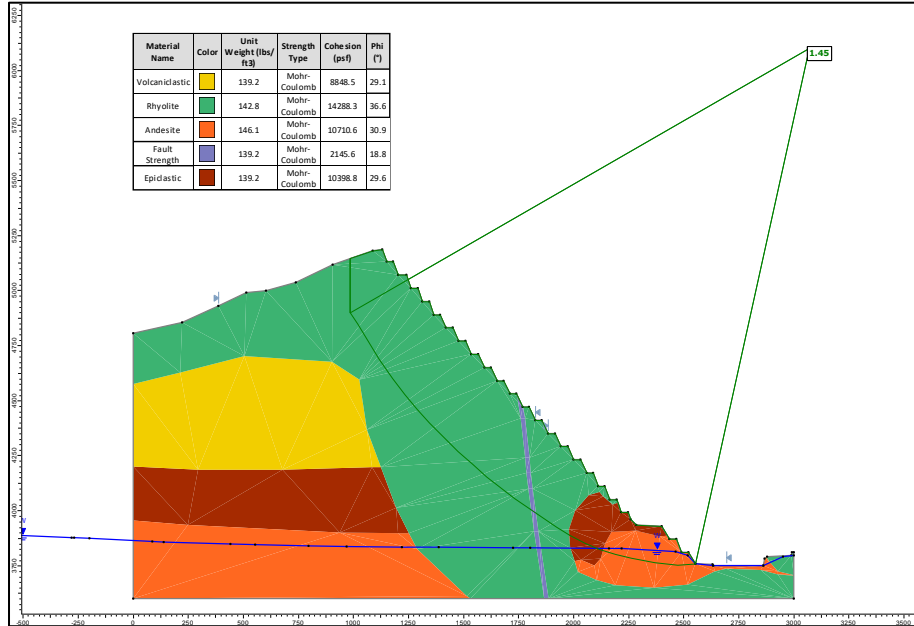


**Figure 3-21. Section 9, Assuming 2036 Water Surface**

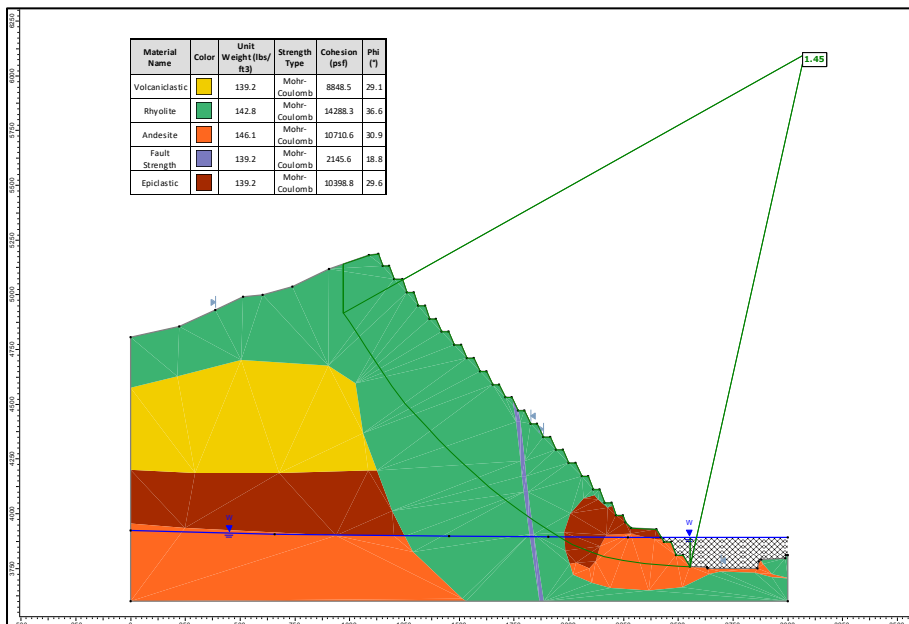


**Figure 3-22. Section 9, Assuming 2023 Water Surface**